Modelling the impact of depositional and diagenetic processes on reservoir properties of the crystal-shrub limestones in the 'Pre-Salt' Barra Velha Formation, Santos Basin, Brazil

Journal Pre-proof

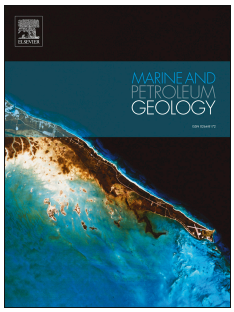

Modelling the impact of depositional and diagenetic processes on reservoir properties of the crystal-shrub limestones in the 'Pre-Salt' Barra Velha Formation, Santos Basin, Brazil

A. Hosa, R.A. Wood, P.W.M. Corbett, R.S. Souza, E. Roemers

PII: S0264-8172(19)30536-7

DOI: https://doi.org/10.1016/j.marpetgeo.2019.104100

Reference: JMPG 104100

To appear in: *Marine and Petroleum Geology*

Received Date: 6 August 2019

Revised Date: 1 October 2019

Accepted Date: 18 October 2019

Please cite this article as: Hosa, A., Wood, R.A., Corbett, P.W.M., Souza, R.S., Roemers, E., Modelling the impact of depositional and diagenetic processes on reservoir properties of the crystal-shrub limestones in the 'Pre-Salt' Barra Velha Formation, Santos Basin, Brazil, *Marine and Petroleum Geology* (2019), doi: https://doi.org/10.1016/j.marpetgeo.2019.104100.

Modelling the impact of depositional and diagenetic processes on reservoir properties of the crystal-shrub limestones in the 'Pre-Salt' Barra Velha Formation, Santos Basin, Brazil

Hosa, A.[1,2], Wood, R. A[1,2*], Corbett, P. W. M. [2,3], Souza, R. S.[4], and Roemers, E.[4]

[1]*School of GeoSciences, University of Edinburgh, James Hutton Road, Edinburgh EH9 3FE, UK*

[2]*International Centre for Carbonate Reservoirs (ICCR)*

[3]*Insitute of Petroleum Engineering, Heriot-Watt University, Riccarton EH14 4AS, UK*

[4]*CENPES, Petrobras, Av. Horácio Macedo, Rio de Janeiro, RJ 21941-598, Brazil*

**Correspondence (Rachel.Wood@ed.ac.uk)*

ABSTRACT

The Cretaceous Barra Velha Formation ('Pre-Salt') of the Santos Basin, Brazil, includes lacustrine crystal-shrub limestones which represent important hydrocarbon reservoirs. Neither single nor multi-phase flow behaviour of these unusual fabrics has been modelled to date. Here we quantify the impact of depositional and diagenetic processes on selected reservoir properties of the crystal-shrub limestones using highly flexible 3D synthetic pore-scale models that can explore parameter space. Rather than producing models validated to actual reservoir properties, this seeks to establish trends and identify emergent clustering behaviour.

Shrubby aggregates nucleate from a surface to form upward and outward-growing, branching, fascicular optical calcite crystal fans that are diverse in size and form. The model allows exploration of the impact of primary growth parameters: number of

bifurcations (or branching), shrub height, angle of cone (or fan) inflation as well as subsequent inter-shrub cementation and dissolution, on resultant porosity, permeability, and multiphase flow.

Simulations show that depositional parameters, as well as two major diagenetic processes - cementation and dissolution - control porosity and permeability. In some cases, these trends diverge considerably from widely-referenced Kozeny-Carman (KC) porosity-permeability relationships. The angle of shrub inflation produces data clusters that traverse KC bands. By contrast, the number of bifurcations and the degree of dissolution follows KC trends, so providing guidance for potential rock type subdivision of similar lithologies. On this basis we propose that the crystal-shrub limestones in the Barra Velha Formation can be subdivided into three broad petrophysical reservoir rock types based on the degree of shrubby aggregate bifurcation and extent of dissolution. The trends explored here can be used to link conceptual and process-based geological models to data, so enabling more accurate prediction and upscaling of heterogeneous reservoir properties and their reservoir-scale distribution.

Keywords: Pre-Salt; Shrubs; Modelling; Permeability; Porosity

INTRODUCTION

Carbonate rocks often show highly heterogeneous and tortuous pore networks compared to simpler granular rocks (such as sandstone) due to the high complexity inherited from both depositional and diagenetic processes. From any starting depositional sediment fabric, many diagenetic pathways involving cementation (porosity loss) and dissolution (porosity enhancement) are possible that lead to a

multitude of final rock types with varying properties. While changes in porosity with cementation and dissolution can be quantified, the corresponding change in permeability is far more complex and difficult to predict as it is controlled by the precise location of cements or the degree of dissolution at the pore scale. Cementation can reduce pore throats as well as increase the surface area and tortuosity of pores, dramatically reducing permeability (Budd, 2001). Dissolution can increase both pore size and pore throats leading to enhanced porosity and pore connectivity (topology) so increasing permeability. Likewise, conversion from porosity to multi-phase flow properties is far from straightforward. Prediction of the distribution of reservoir quality in carbonate rocks therefore requires an understanding of the evolution of depositional and diagenetic controls on porosity creation and occlusion.

Here we quantify the relationship between major controls on the genesis of the pore system and the emergent fluid flow properties of the crystal-shrub limestones of the Barra Velha Formation. These distinctive 'Pre-Salt' carbonate lithologies formed in non-marine, lacustrine settings, and now host some of the most globally volumetrically-significant hydrocarbon reservoirs in the offshore Santos Basin, Brazil (Figure 1). To date, no modelling has been undertaken to quantify either single or multiphase flow behaviour of these unusual facies.

GEOLOGICAL SETTING

The Barra Velha Formation comprises a unique Cretaceous (Aptian), non-marine, Pre-Salt sedimentary succession of continental carbonate and non-carbonate rocks intercalated with volcanic basaltic rocks, which formed along the Brazilian margin of the South Atlantic during rifting and the breakup of Gondwana (Figure 1; Abrahao and Warme, 1990; Karner and Gamboa, 2000). Broadly similar litholgies are known

from the Kwanza and Namibe basins in the conjugate margin of Angola (Figure 1A; Shroeder et al., 2015; Saller et al. 2016). The Barra Velha Formation sequence is mostly composed of lacustrine autochthonous and allochthonous sedimentary rocks, where the autochthonous component formed by both abiogenic and biogenic processes within a hydrothermal evaporitic environment (Rezende and Pope, 2015; Saller et al., 2016). Dominantly abiogenic lithologies include bedded shrub-like limestones, bedded travertines, Mg-rich argillaceous chemical sediments with spherulitic calcite crystals, and laminites, whereas the primarily biogenic group is composed of laminated microbial boundstones (Souza et al., 2018).

Carbonate lithologies may have formed platforms and mounds on tectonically-induced palaeo-highs (Ceraldi and Green, 2017; Saller et al., 2016; Wright and Barnett, 2015). The presence of underlying volcanic basement and alkaline lake chemistry with high pH and silica concentration created these highly unusual, hetergeneous, and complex lithologies, which show a complex and poorly understood relationship between depositional and diagenetic processes (Tosca and Wright, 2015). Variations between the characteristic shrubby calcite, spherulitic calcite crystals, and laminar facies are believed to be a result of the interactions between pH, magnesium clays, hydraulic conditions, and possibly microbial activity (Wright and Barnett, 2015; Saller et al., 2016; Ceraldi and Green, 2017). As with some alkaline lakes in east Africa, slight increases in pH could also trigger silica precipitation, which may have been partly mediated by microbes (Saller et al., 2016). An evaporative model has been proposed, where aligned crystal beds form at the sediment-water interface interbedded with laminate facies within a closed, saline, basin (Farias et al., 2019).

CRYSTAL-SHRUB FACIES

The shrub-like limestones, the subject of this work, are composed of dense radiating fibrous calcitic crystal aggregates of tabular crystals a few mm in length, which form multiple layers of bifurcating shrubs of diverse width and height (here termed shrubs, or shrubby aggregates; Figure 2a and b). These are generally mm-cm sized but up to 1-3 cm in width and often mm-cm but up to dm in height, which typically showing irregular, upward and outward-expanding branching growth. Individual shrubs are composed of acicular crystals recrystallized as fascicular optical calcite aggregates, with sweeping extinction (Souza et al., 2018). These precipitates generate a growth-framework primary pore system with moderate porosity and good permeability, controlled by large pore throats (Herlinger et al., 2017). It is proposed that shrub size, sorting, and packing, in particular the size of individual shrubs, exerts a primary control on pore size, affecting both porosity and permeability (Rezende and Pope, 2015). These Pre-Salt crystal shrub fabrics have been widely compared to Modern and Pleistocene dendritic travertines (e.g. Claes et al. 2017).

The crystal-shrub limestones are characterized by multiple phases of calcite, dolomite and quartz cements sitting adjacent to and/or replacing the primary authigenic carbonates, as well as multiple phases of dissolution (Figure 2c; Chitale et al., 2015; Saller et al., 2016; Herlinger et al., 2017; Lima and De Ros, 2019; Souza et al., 2018; Farias et al., 2019). Saddle-dolomite, dawsonite, celestine, and barite occur locally, with dolomite being a major source of primary porosity occlusion (Herlinger et al., 2016; Souza et al., 2018; Farias et al., 2019). While these diagenetic processes are known to be important determinants of reservoir properties, creating highly heterogeneous changes in porosity and permeability over several orders of magnitude

(Herlinger et al., 2017; Terra et al., 2010), the impact of each control has not been isolated or quantified.

PORE-SCALE MODELLING

Microfocus Computer Tomography (μCT) is used to generate 3D images of pore space, but carbonate pore systems can contain submicron features which lie below the resolution of μCT scans, so this method often fails to capture the complete pore system, with its multi-scale pore-size distribution and connectivity over several orders of magnitude (Knackstedt et al., 2004). More importantly, given the absence of significant density contrast, μCT scan images may not accurately discriminate between depositional and diagenetic products in carbonate rocks. Such scans do not produce flexible models, and so cannot be used to explore the range of hypothetical primary and diagenetic parameter combinations possible.

Pore-scale modelling combined with the Lattice Boltzmann method to simulate three-dimensional flow at the pore scale has been widely used to predict carbonate reservoir rock properties such as absolute permeability, capillary pressure, and relative permeability. Such models are often based either on μCT scans (e.g. Soete et al., 2017), statistical reconstruction (see Okabe and Blunt, 2007; Roth et al., 2011; van de Land et al., 2013), or process-based modelling (Biswal et al. 2007; Lander et al. 2008; Mousavi et al., 2012; Harland et al., 2015; Hosa and Wood, 2017). The advantage of synthetic rock models is that, although they may be of relatively low resolution, they are flexible and considerably less expensive than data obtained via laboratory measurement, and can enable exploration of variability in controlling parameters. While synthetic models may not create accurate absolute values, their flexibility enables isolation and quantification of the effect of a particular depositional

and diagenetic processes and products, and so can establish trends and test hypotheses as to how different depositional and diagenetic factors influence reservoir properties.

To date, while the petrophysical response of the Pre-Salt has been interrogated (e.g. see Alabi et al., 2014), no pore-scale modelling has been undertaken on the shrubby Pre-Salt lithologies, to understand the major controls on either single or multiphase flow. New empirical methods for understanding the interaction of complex pore behaviours have been proposed using multi-layer static and dynamic petrophysical models based on well log and core data (Diniz-Ferreira and Verdin, 2012). The petrophysical properties of modern shrubby travertines with similarly highly complex pore networks have also been investigated as Pre-Salt analogues (e.g. Claes et al., 2017).

Here we create highly flexible 3D synthetic pore-scale object-based models to explore a far greater range of realistic but hypothetical morphologies in order to quantify the relationship of depositional and diagenetic features to emergent single and multiphase fluid flow properties of the crystal-shrub limestones of the Barra Velha Formation.

METHODOLGY

Depositional and diagenetic features of 3D synthetic shrub facies are modelled using a modified version of Calcite3D (Hosa and Wood, 2017). Calcite3D is a Matlab object-based model that simulates cementation in natural carbonates, taking into account the geometries of the evolving cements, as well as local effects such as grain impingement. This approach to modelling is geometric and object-based, and so focuses on recreation of approximate shapes characteristic of all significant elements. Our model is fully flexible and implemented in 3D, so enabling more accurate

modelling of flow properties than 2D models. Here this model is expanded to create shrub depositional fabrics, and to include two further diagenetic processes: crust-like, isopachous, fringing carbonate cement, and a phase of crystal aggregate or cement crust dissolution (Figure 3).

From the generated 3D models of the pore structure a geometrical/topological network can be extracted (Jiang et al., 2007, 2011) consisting of pore bodies (nodes) and pore throats (bonds). Pore-throat radius distribution, and the average connectivity or topology of a rock (Euler number), can be derived from the extracted network. In pore networks the (specific) Euler number is the number of nodes minus the number of bonds (divided by the rock volume). The Euler number can be used to derive a pore size dependent connectivity function by removing pores from the network in order of increasing size and recalculating the Euler number at each step (Vogel and Roth, 2001). Removing larger and larger pores will eventually result in a positive Euler number (i.e. fewer bonds than nodes), which indicates the point at which the network becomes disconnected. As such, an Euler number of zero is a proxy for the percolation radius of the network.

The network flow model used (Pore Analysis Tools, or PATs) captures the physics of single and multi-phase flow at the pore scale to calculate continuum-scale flow properties (Van Dijke and Sorbie, 2006; Ryazanov et al., 2009; Pak et al., 2016). Horizontal permeability (parallel to bedding) is modelled. For the phase relative permeabilities, the pressure distribution is computed for each phase in response to a pressure gradient applied to the given phase at given saturation increments. Two-phase characteristics are predicted by simulating primary drainage and water invasion. We present multi-phase fluid flow results from shrub rock textures that explore different depositional models and stages of diagenesis. The overall goal is to establish

trends in the evolution of porosity and permeability and multiphase flow characteristics in response to depositional variability and different diagenetic events (Table 1).

First, we explore the major depositional parameters that determine shrub growth (Terra et al. 2012; Saller et al., 2016; Herlinger et al., 2017). Shrubs often grow nucleated from spherulites, and may have several generations of branches (following multiple bifurcations), and each set can have variable height (typically 5-10 mm). Shrub size also varies in the angle of inflation of the crystal fan (cone) from nucleation. The published variation is modelled in the average distance between nucleation sites (1.5-2 mm), the size of shrub cone inflation (angles of 20^o, 25^o, 30^o and 35^o), shrub height (6 and 9 mm), and the number of shrub generations (1, 2 and 3; Figures 4 and 5; Table 1). Models are 18^3 mm, and 360^3 voxels.

Second, two major diagenetic events on the synthetic shrubs are modelled: crust-like carbonate cement and dissolution. The output of the depositional model is voxelised to a size of 360^3 voxels at a resolution of 50 μm, and cementation is implemented in Calcite3D to grow cement on all primary, inter-shrub, porosity of the synthetic shrubs. Sensitivity analysis of models with a voxel size of 10 μm and a computational domain size of 300^3 demonstrates that at that resolution porosity as well as permeability are stable (Hosa and Wood, 2017).

Cementation (c) is modelled as an isopachous crust 100 μm thick (Figure 6). A layer of cement is added in one step around all inter-shrub porosity. For simplicity, all pores develop cement equally. Dissolution is implemented with two parameters: the depth of dissolution (ad), and the percentage of solids removed (asp) within this zone of dissolution to create a more realistic local patchiness or heterogeneity of dissolution (Figure 7). Dissolution is implemented as removal of the solid material by

turning all solid voxels inside 'dissolving radius' of any pore into pore. The depth of dissolution (ad) modelled was 100 µm, 150 µm and 200 µm. The percentage of solids removed (asp) within these dissolution zones was 40%, 50% and 60% (Figure 7).

Multiple model outputs (synthetic samples) were generated for combinations of the 6 shrub modelling parameters: cone angle (4 values), bifurcation level (3 values), height (2 values), distance between nucleation sites (2 values), dissolution depth (3 values) and dissolution percentage (3 values). One sample was generated for each combination of interest amounting to a total for each of between 48-240 generated samples. Models were generated until trends became clear.

Empirical porosity-permeability (poroperm) relationships, such as the Kozeny-Carman (KC) equation (Kozeny, 1927; Carman, 1937), are widely used to relate porosity to permeability, and sometimes to predict permeability from porosity:

$$\kappa = \frac{1}{cS^2} \cdot \frac{\phi^3}{(1-\phi)^2} \qquad (1)$$

where κ is the permeability, ϕ is the porosity, c is the Kozeny constant and S is the specific surface area.Here we compare our model outputs to the porosity-permeability fields expressed as Global Hydraulic Elements (GHE) (Corbett and Potter, 2004), defined by curves based on the KC equation and having the following form:

$$\kappa = \frac{FZI^2}{0.0314^2} \cdot \frac{\phi^3}{(1-\phi)^2} \qquad (2)$$

where κ is the permeability, ϕ is the porosity (fractional) and FZI is the Flow Zone Indicator. In the GHE framework, a regular series of FZI values (an exponential series in permeability space) based on a simple progression is selected to define different fields of shared petrophysical characteristics where data can be clustered. When these fields follow model data that explores a given parameter, trends can convey geological significance.

RESULTS

Results are presented in terms of several quantities of interest (Table 1). These are the angle of shrub cone inflation (a), shrub height (h), the number of shrub bifurcations (branches, b), cementation thickness (c), depth of dissolution (ad), percentage of solids removed (asp), pore-size-distribution (PSD), connectivity (Euler number, the number of pores minus the number of pore throats per volume (Jiang et al., 2017, 2012), drainage capillary pressure (Pc), drainage relative permeability (Kr), porosity (ϕ), permeability (κ), and Global Hydraulic Elements (GHE) curves. Results are shown following a scheme where the notation of different porosity-permeability fields (GHEs) follows 9, 10, 10a-10e (Corbett and Potter, 2004). The behaviour of the models within the GHEs is then discussed in terms of defining petrophysical reservoir rock types (RRTs), based on shared flow behaviour.

Models result in highly variable porosity and permeability, ranging from 1.3-33.4 % and 20-12,000 D.

Impact of primary growth parameters

Progressively wider angle of shrub cone inflation decreased drainage capillary pressures (Pc) and the number of larger pores as shown by the pore size distribution, as well as reducing connectivity, and created more shallow relative permeability curves (Kr) (Figure 8). The Euler number passes through zero at successively higher pore sizes in the pathways with narrower cone growth angles showing that the network is becoming more unconnected at smaller pore sizes. Comparison of porosity and permeability shows that each modelled shrub cone growth angle forms a discrete cluster with little overlap and each of which transect across three to five GHE curves.

20^o shrub cones creates the highest porosity and permeabilities, with a range of porosity and permeability from 5.7-33.4 % and 970-12,000 D; 25^o shrub cones range from 3.6-23.8 % to 500-7,900 D; 30^o shrub cones range from 2.0-18.6 % to 120-4200 D, and 35^o shrub cones show the lowest values ranging from 1.3-15.7 % to 20-1,500 D, respectively.

The number of shrub bifurcations (b), showed that succesive branching increased drainage capillary pressures but decreased the number of larger pores, increased connectivity, and created steeper relative permeability curves (Figure 9). The Euler number passes through zero at successively higher pore sizes in the pathways with increased numbers of shrub bifurcations showing that the network is becoming more unconnected at smaller pore sizes. Porosity and permeability plots show that the three shrub generations styles form discrete clusters that each follow one to two GHE curves. Non-bifurcated shrub (1) follows 10d and e; shrub with one bifurcation (2) follows 10c, and shrubs with two shrub bifurcations (3) follows 10a and b.

Variation in shrub height did not create any distinct trends or clustering of any reservoir flow characteristics (Figure 10).

Impact of diagenetic parameters

Variations in the depth of dissolution (ad) showed that increasing depth increased drainage capillary pressures and the number of larger pores, as well as connectivity, and created steeper relative permeability curves (Figure 11). The Euler number passes through zero at successively higher pore sizes in the pathways with increasing depths of dissolution showing that the network is becoming more unconnected at smaller pore sizes. Porosity and permeability plots for each depth of dissolution form

discrete clusters which follow one to two GHE curves:100 µm follows 10d; 150 µm follows 10c; and 200 µm follows 10a and b.

Variations in the percentage of dissolution (asp) parameter did not create any distinct trends or clustering of reservoir flow characteristics, except that increasing percentage dissolution increased drainage capillary pressures (Figure 12).

DISCUSSION

Limitations of the model

While our models are successful in modelling realistic changes in cement volumes and pore space morphology, modelled permeabilities (2-1,200 D) are markedly higher than the 4.2D (Diniz-Ferreira and Verdín, 2012; Herlinger et al., 2016). This is due primarily to the very high permeability of the initial synthetic primary deposit (although this was not simulated here) and the low resolution of the models (50 µm). The shrub depositional models also have only few points of contact so that the narrowest portions of pore throats are effectively very short so creating relatively large primary, inter-shrub pore spaces, yielding very high porosities and permeabilities.

There is always a trade-off between model size and resolution. Our models are of relatively low resolution and do not capture all porosities, in particular microporosity such as intracrystalline pores within the shrub. Models have a size of 18 mm^3 with a resolution of 50 µm, so are limited to a relatively small number of shrubs as well as to the accuracy of the voxel representation of the shrubs. Realistic pore throat sizes cannot often be captured as small and/or thin pore throats can also be lost due to segmentation, which results in a loss of sub-resolution pore connectivity, so influencing the quality of permeability prediction. Likewise, it is unlikely that

representative elementary volume (REV; the smallest volume over which a measurement can be made which yields a value representative of the whole) have been captured in these models (see Claes et al., 2017). But to do so would have excessively compromised the model resolution such that the only pore space captured would be very large macropores.

We model only relatively simple diagenetic processes, even though diagenesis of the Pre-Salt lithologies is highly complex (Herlinger et al., 2017; Lima and De Ros, 2019). We limit cementation to a thickness of 100 µm, as in theory this can proceed to occlude all primary pore space. We also do not take mechanical compaction into account, but this is limited in these Pre-Salt lithologies (Saller et al., 2016). In addition, in the Pre-Salt shrub reservoir lithologies, there is an additional complexity of the local occurrence of Mg-silicate clays and associated diagenetic products, which have not been modelled here.

Trends of flow behaviour

Notwithstanding limitations of the modelling methodology, we can establish *trends* and identify clustering behaviour of reservoir properties with *changes* in major depositional and diagenetic parameters, i.e. petrophysical trends that have a geological, process-based significance. Poroperm data generated indeed exhibits a linear relationship between the logarithms of porosity and permeability with a high coefficient of determination, as observed in natural media. The data can be fitted with a linear function of the logarithms of porosity and permeability, demonstrating a clear pattern with little variation in the synthetic data.

Not surprisingly, porosity-permeability outputs from all models result in very different trends compared to those modelled from a range of simple, cemented

grainstones (Hosa and Wood, 2017). Our models confirm trends gained from petrophysical plug data that shows that primary growth-framework primary pore system of the crystal shrubs was controlled by large pore sizes, and that partial dissolution of shrubs and cements increased porosity and has led to an enlargement of pore size, with a consequent increase of permeability (Herlinger et al., 2017).

Simulations show that all depositional parameters, cementation, and dissolution control porosity and permeability. The trends in poroperm output from most explored parameters follows standard Kozeny-Carman (KC) porosity-permeability relationships. This is noteworthy, as similar model outputs for a range of cemented grainstones diverged considerably from KC relationships (Hosa and Wood, 2017).

We can establish which parameters have the greatest impact on flow behaviour. Variation in shrub height may in part determine the degree of vertical connectivity. Although there are no discernible predictable control over multiphase flow behaviour (Figures 10A, B, D, and E), the shorter shrubs show the highest modelled absolute horizontal permeabilities and porosities (Figure 10C). An increasing shrub cone angle and increased number of bifurcations both markedly decrease reservoir quality. By contrast, an increased depth of dissolution notably increases reservoir quality.

The angle of shrub cone inflation produce poroperm data clusters that traverse KC bands. By contrast, the number of bifurcations and the degree of dissolution follow KC trends, so providing guidance for potential subdivision of models into groups with shared reservoir properties (rocktypes).

Reservoir Rock Types

On this basis we propose that shrub facies in the Barra Velha Formation can be subdivided into three broad petrophysical rocktypes based on the degree of shrub

bifurcation and extent of dissolution. Two shrub bifurcations combined with a high degree (200 μm) of dissolution yield rocktypes that follow GHE 10a and b; one shrub bifurcations combined with a medium degree (150 μm) of dissolution yield rock types that follow GHE 10c, and no shrub bifurcations combined with a low degree (100 μm) of dissolution yield rock types that follow GHE 10d.

Conclusions

While combined multiscale petrophysical and geological data may be needed to capture all textural and flow heterogeneities in the Pre-Salt shrub lithologies, the trends established with the use of our hypothetical models can be compared with those derived from real core plug measurements to help understand controls on poroperm variation, place expensive laboratory measurements within an appropriate geological context, and improve partitioning of data to guide and model permeability prediction.

Most importantly, the trends explored here can be used to link conceptual and process-based geological models to data, so enabling more accurate prediction and upscaling of reservoir properties and their reservoir-scale distribution. In particuar, we show that an increase in shrub height decreases reservoir quality, but the number of bifurcations and depth of dissolution notably increases reservoir quality. As such, these models can help to predict the flow behaviour of these highly heterogenous carbonates as they can be tied to primary depsoitional and diagenetic variation both vertically and horizontally, and on multiple length scales.

ACKNOWLEDGEMENTS

We acknowledge the support of Petrobras and Shell for financial support of the International Centre for Carbonate Reservoirs (ICCR), as part of the Rocktype II project. We are grateful for management support from Frances Abbots (Shell) and Jorge-Andre Bras (Petrobras), and technical input from Conxita Taberner and Andrew Barnett. We are grateful to Rink van Dijke for his comments.

REFERENCES

Abrahao, D., and Warme, J.E., 1990, Lacustrine and Associated Deposits in a Rifted Continental Margin - Lower Cretaceous Lagoa Feia Formation, Campos Basin, Offshore Brazil. In Katz, B.J (ed.) Lacustrine Basin Exploration: Case Studies and Modern Analogs: *AAPG Memoir*, v. 50, p. 287-305.

Alabi, G., Kasten, R., Chitale, V., Yadavalli, S., and Piccoli, L., 2014, The value of petrophysical measurements across multiple scales. A lacustrine carbonate example from Campos Basin, Brazil. In: SPWLA 55th Annual Logging Symposium, pp. 1e12.

Biswal, B., Øren, P. E., Held, R. J., Bakke, S., and Hilfer, R., 2007, Stochastic multiscale model for carbonate rocks: *Physical Review E*, v. 75, p. 061303.

Blunt, M. J., Bijeljic, B., Dong, H., Gharbi, O., Iglauer, S., Mostaghimi, P., Paluszny, A., and Pentland, C., 2013, Pore-scale imaging and modelling: *Advances Water Research*, v. 51, p. 197– 216.

Budd, D. A., 2001, Permeability loss with depth in the Cenozoic carbonate platform of west-central Florida: *AAPG Bulletin*, v. 85, p. 1253–1272.

Carman, P.C., 1937, Fluid flow through granular beds: *Transactions, Institution of Chemical Engineers, London*, v. 15, p. 150-166.

Ceraldi, T.S. and Green, D., 2017, Evolution of the South Atlantic lacustrine deposits

in response to Early Cretaceous rifting, subsidence and lake hydrology. In Sabato Ceraldi, T., Hodgkinson, R. A. and Backe, G. (eds) Petroleum Geoscience of the West Africa Margin. *Geological Society, London, Special Publications,* v. 438, p.77-98.

Chitale, V.D.V., Alabi, G., Gramin, P., Lepley, S., and Piccoli, L., 2014, Reservoir characterization challenges due to the multiscale spatial heterogeneity in the Presalt carbonate Sag formation, North Campos Basin, Brazil: SPWLA-2015-v56n6a1

Claes, H., Erthal, M.M., Soete, J., Ozkul, M., and Swennen, R., 2017, Shrub and pore type classification: petrography of travertine shrubs from the Ballik–Belevi area (Denizli, SW Turkey): *Quaternary International*, v. 437, p. 147–163.

Corbett, P. W. M., and Potter, D. K., 2004, Petrotyping: a basemap and atlas for navigating through permeability and porosity data for reservoir comparison and permeability prediction: *International Symposium of the Society of Core Analysts*, SCA2004-30, p. 5-9.

Diniz-Ferreira, E.L. and Verdin, C.T, 2012, Improved estimation of pore connectivity and permeability in deepwater carbonates with the construction of multi-layer static and dynamic petrophysical models: SPWLA 53rd Annual Logging Symposium.

Erthal, M.M., Capezzuoli, E., Mancini, A., Claes, H., Soete, J., and Swennen, R., 2017, Shrub morpho-types as indicator for the water flow energy - Tivoli travertine case (Central Italy): *Sedimentary Geology*, v. 347, p.77-99.

Farias, F., Szatmari, P., Bahniuk, A., and Barros França, A., 2019, Evaporitic carbonates in the pre-salt of Santos Basin – Genesis and tectonic implications: *Marine and Petroleum Geology*, v. 105, p. 251-272.

Harland, S., Wood, R., Curtis, A., van Dijke, M.I., Stratford, K., Jiang, Z., Kallel, W., and Sorbie, K., 2015, Quantifying flow in variably wet microporous carbonates using object-based geological modelling and both lattice-Boltzmann and pore network fluid flow simulations: *AAPG Bulletin,* v. 99, p. 1827–1860.

Herlinger, RR., Zambonato, E.E., and de Ros, L.F., 2017, Influence of diagenesis on the quality of lower cretaceous Pre-salt lacustrine carbonate reservoirs from northern Campos basin, offshore Brazil: *Journal of Sedimentary Research,* v. 87, p. 1285–1313.

Hosa, A., and Wood, R., 2017, Quantifying the impact of early calcite cementation on the reservoir quality of carbonate rocks: a 3D process-based model: *Advances in Water Resources,* v. 104., p. 89-104.

Jiang, Z., Wu, K., Couples, G.S, van Dijke, M.I.J., Sorbie, K.S., and Ma, J., 2007, Efficient extraction of networks from three-dimensional porous media: *Water Resources Research*, **v.** 43**,** p. W12S03.

Jiang, Z., van Dijke, M.I.J., Wu, K., Couples, G.D., Sorbie, K.S., and Ma, J., 2012, Stochastic pore network generation from 3D Rock Images: *Transport in Porous Media,* v. 94, p. 571-579.

Karner, G.D. and L.A.P. Gambôa, 2007, Timing and origin of the South Atlantic pre-salt sag basins and their capping evaporites. In: Schreiber, B.C., Lugli, S., and Babel, M. (eds.), Evaporites through space and time. *Geological Society of London, Special Publication,* v. 285, p.15-35.

Kozeny, J., 1927, Ueber kapillare Leitung des Wassers im Boden: *Sitzungsberger Akademie Wissenschaft Wien,* v. 136, p. 271-306.

Knackstedt, M.A., Arns, C.H., Limaye, A., Sakellariou, A., Senden, T.J., Sheppard,

A.R., Sok, R.M., Pinczewski, W.V., and Bunn, G.F., 2004. Digital core laboratory: reservoir-core properties derived from 3D images*: Journal of Petroleum Technology*, v. 56, pp. 66-68.

Lander, R., Larese, R., and Bonnell, L., 2008, Toward more accurate quartz cement models: The importance of euhedral versus noneuhedral growth rates: *AAPG Bulletin*, v. 92, p. 1537–1563.

Lima, B.E.M., and De Ros, L. F., 2019, Deposition, diagenetic and hydrothermal processes in the Aptian Pre-Salt lacustrine carbonate reservoirs of the northern Campos Basin, offshore Brazil: *Sedimentary Geology*, v. 383, p. 55-81.

Moreira, J.L.P., Madeira, C.V., Gil, J.A., and Machado, M.A.P., 2007, Bacia de Santos*: Bolletin Geociencias Petrobras*, v.15, p. 531–549.

Mousavi, M. A., Prodanovic, M., and Jacobi, D., 2012, New classification of carbonate rocks for process-based pore-scale modeling: *Society of Petroleum Engineers*, 18, doi:10.2118/163073-PA.

Okabe, H., and Blunt, M. J., 2007, Pore space reconstruction of vuggy carbonates using microtomography and multiple-point statistics: *Water Resources Research*,v. 43, doi:10.1029/2006WR005680.

Pak, T., Butler, I., Geiger, S., van Dijke, M, I, J., Jiang , Z., and Surmas, R., 2016, Multiscale pore-network representation of heterogeneous carbonate rocks: *Water Resources Research*, v. 52, p. 5433-5441.

Pereira, A., Dos Santos, E., Silva, E., Leite, K., Tritlla, J., Ayres, H., and Machin, J., 2013, Santos Microbial Carbonate Reservoirs: A Challenge, Paper OTC-24446 presented at Offshore Technology Conference Brasil, Rio de Janeiro, Brazil, 29–31 October. DOI: http://dx.doi.org/10.4043/24446 MS.

Rezende, M.F., and Pope, M.C., 2015, Importance of depositional texture in pore

characterization of subsalt microbialite carbonates, offshore Brazil. *Geological Society of London, Special Publication,* v. 418, p. 193-207.

Roth, S., Biswal, B., Afshar, G., Held, R. J., Øren, P.-E., Inge Berge, L., and Hilfer, R., 2011, Continuum-based rock model of a reservoir dolostone with four orders of magnitude in pore sizes: *AAPG Bulletin*, v. 95, p. 925–940.

Ryazanov, A.V., van Dijke, M.I.J. and Sorbie, K.S. 2009, Two-Phase Pore-Network Modelling: Existence of Oil Layers During Water Invasion: *Transport in Porous Media* v**.** 80, p. 79-85.

Saller, A., Rushton, S., Buambua, L., Inman, K., McNeil, R., and Dickson, J.A.D., 2016, Presalt stratigraphy and depositional systems in the Kwanza Basin, offshore Angola: *AAPG Bulletin* v. 100, p. 1135–1164.

Shroeder, S., Ibekwe, A., Saunders, M., R. Dixon, R. and Fisher, A., 2015, Algal–microbial carbonates of the Namibe Basin (Albian, Angola): implications for microbial carbonate mound development in the South Atlantic: *Petroleum Geoscience*, v. 22, pp 71-90.

Soete, J., Claes, S., Janssens, N., Cnudde, V., Huysmans, M., and Swennen, R., 2017, Lattice Boltzmann simulations of fluid flow in continental carbonate reservoir rocks and in upscaled rock models generated with multiple-point geostatistics: *Geofluids*, v. 2017, Article ID 7240524.

Souza, R.S., Arienti, L.M., Viana, S.M., Falcão, L.C., Cuglieri, M.A., Silva Filho, R.P., Leite, C.O., Oliveira, V.C., Oliveira, D.M., Anjos, C., Amora, R., Carmo, I.D., Coelho, C.E., 2018, Petrology of the Hydrothermal and Evaporitic Continental Cretaceous (Aptian) Pre-salt Carbonates and Associated Rocks, South Atlantic Santos Basin, Offshore Brazil: *AAPG Annual Convention, Salt Lake City.*

Terra, G.J.S., Spadini, A.R., Franca, A.B., Sombra, C.L., Zambonato, E.E., Juschaks, L.C.S., Arienti, L.M., Erthal, M.M., Blauth, M., Franco, M.P., Matsuda, N.S., Da Silva, N.G.C., Moretti, P.A., Jr., D'Avila, R.S.F., De Souza, R.S., Tonietto, S.N., Dos Anjos, S.M.C., Campinho, V.S., and Winter, W.R., 2010, Carbonate Rock Classification Applied to Brazilian Sedimentary Basins: *Boletin de Geosciencias de Petrobras*, v. 18, p. 9–29.

Tosca, N.J. and Wright, V.P., 2015, Diagenetic pathways linked to labile Mg-clays in lacustrine carbonate reservoirs: a model for the origin of secondary porosity in the Cretaceous pre-salt Barra Velha Formation, offshore Brazil. In Armitage, P. J., Butcher, A. R., Churchill, J. M., Csoma, A. E., Hollis, C., Lander, R. H., Omma, J. E. & Worden, R. H. (eds) Reservoir Quality of Clastic and Carbonate Rocks: Analysis, Modelling and Prediction: *Geological Society, London, Special Publications*, v. 435, p. 33-46.

Van der Land, C., Wood, R., Wu, K., van Dijke, M. I., Jiang, Z., Corbett, P. W. M., and Couples, G., 2013. Modelling the permeability evolution of carbonate rocks: *Marine and Petroleum Geology* v. 48, p. 1- 7.

van Dijke, M. I..J., and Sorbie, K.S., 2006, Existence of fluid layers in the corners of a capillary with non-uniform wettability: *Journal Colloid and Interface Science* v. 293, p. 455–463.

Vogel, H.J., and Roth, K., 2001, Quantitative morphology and network representation of soil pore structure: *Advances in Water Resources* v. 24, p. 233-242.

Wright, V. P., and Barnett, A., 2015, An abiotic model for the development of

textures in some South Atlantic early Cretaceous lacustrine carbonates. In: Bosence, D. W. J., Gibbons, K. A., Le Heron, D. P., Morgan, W. A., Pritchard, T. and Vining, B. A. (eds) Microbial Carbonates in Space and Time: Implications for Global Exploration and Production: *Geological Society, London, Special Publications*, v. 418, p. 209–219.

Table and Figure captions

Table 1: Primary (depositional) and diagenetic parameters used in pore-scale modelling.

Figure captions

Figure 1: Geological setting. **A**: Map of the South Atlantic showing major Cretaceous 'Pre-Salt' basins; **B**: Stratigraphy of the Lower Cretaceous of the Santos Basin, Brazil, with the Barra Velha Formation highlighted (modified from Moreira et al., 2007).

Figure 2: Major primary and diagenetic features of crystal-shrubs. **A**: Plane polarised photomicrograph of longitudinal section showing primary features of nucleation and bifurcation (branching); **B**: Cross-polarised photomicrograph of same area, showing dense radiating fibrous calcitic crystal aggregates; **C**: Cathodoluminescence image of longitudinal section showing multiple cementation (dolomite and calcite) and dissolution events. Arrows indicate way-up.

Figure 3. Modelling methodology. **A**: Crystal shrub growth parameters are used to model 3D synthetic shrub; **B**: Transverse section of the synthetic deposit is discretised and cropped to avoid artefacts in grain arrangement due to box boundaries, shown here in 2D (pore space on white); **C**: Multiphase flow simulation using Pore Analysis Tools (PATs) to test effect of depositional parameters; **D**: Transverse section showing cement crust growth is simulated using Calcite 3D (pore space in white); **E**. Implementation of velocity-based dissolution using Calcite 3D; **F**: Multiphase flow simulation using PATs to test effect of diagenetic parameters. Adapted from Hosa and Wood (2017).

Figure 4: Shrub growth parameters, and typical 3D output of a single shrub that was allowed to grow without obstruction, i.e. other impinging shrubs.

Figure 5: Shrub growth model. Models of multiple generations of 3D shrubs, with selected cross-sections showing pore (white) and solid (black) demonstrating the horizontal-vertical heterogeneneity.

Figure 6. Cementation model. Cross section through a 100^3 portion of the full 360^3 3D model of grown shrub (black) without cement (upper), and with cement (blue, lower), with porosity of full 3D models. Starting and final porosities are shown of the full 3D models.

Figure 7. Dissolution model. Cross sections through a 100^3 portion of the full 360^3 3D model of grown shrub (black) with stages of dissolution (red). The two parameters used the depth of dissolution (ad), and percentage of solids removed within the zone

of dissolution (asp). Starting and final porosities are shown of the full 3D models that follow a stage of 100 μm (ad), followed by the full range of (asp).

Figure 8: Reservoir properties for different angles of crystal shrub cone inflation (ang), for final expressions of 48-240 model outputs. **A**: Drainage capillary curves; **B**: Changes in pore size distribution (PSD); **C**: Poroperm of model output plotted against a background of Global Hydraulic Elements curves (GHE), based on Kozeny-Carman (KC), as defined by Corbett and Potter (2004). These data fall into four clusters that traverse GHE curves; **D**: Relative permeability curves; **E**: Connectivity as expressed by Euler number (the number of nodes (or pores) minus the number of bonds (or pore throats) divided by the volume of the model).

Figure 9: Reservoir properties for different crystal shrub bifurcation (branch), for final expressions of 48-240 model outputs. **A**: Drainage capillary curves; **B**: Changes in pore size distribution (PSD); **C**: Poroperm of model output are plotted against a background of Global Hydraulic Elements curves (GHE), based on Kozeny-Carman (KC), as defined by Corbett and Potter (2004). These data fall into three clusters that follow GHE curves; **D**: Relative permeability curves; **E**: Connectivity as expressed by Euler number (the number of nodes (or pores) minus the number of bonds (or pore throats) divided by the volume of the model).

Figure 10: Reservoir properties for different crystal shrub height (h), for final expressions of 48-240 model outputs. **A**: Drainage capillary curves; **B**: Changes in pore size distribution (PSD): **C**: Poroperm of model output are plotted against a background of Global Hydraulic Elements curves (GHE), based on Kozeny-Carman

(KC), as defined by Corbett and Potter (2004). These data fall into two clusters that follow GHE curves; **D**: Relative permeability curves; **E**: Connectivity as expressed by Euler number (the number of nodes (or pores) minus the number of bonds (or pore throats) divided by the volume of the model).

Figure 11: Reservoir properties for different depths of dissolution (ad), for final expressions of 132-144 model outputs. **A**: Drainage capillary curves; **B**: Changes in pore size distribution (PSD); **C**: Poroperm of model output are plotted against a background of Global Hydraulic Elements curves (GHE), based on Kozeny-Carman (KC), as defined by Corbett and Potter (2004). These data fall into three clusters that follow GHE curves; **D**: Relative permeability curves; **E**: Connectivity as expressed by Euler number (the number of nodes (or pores) minus the number of bonds (or pore throats) divided by the volume of the model).

Figure 12: Reservoir properties for different percentages of dissolution (asp), for final expressions of 144 model outputs. **A**: Drainage capillary curves; **B**: Changes in pore size distribution (PSD); **C**: Poroperm of model output are plotted against a background of Global Hydraulic Elements curves (GHE), based on Kozeny-Carman (KC), as defined by Corbett and Potter (2004). These data fall into three clusters that follow GHE curves; **D**: Relative permeability curves; **E**: Connectivity as expressed by Euler number (the number of nodes (or pores) minus the number of bonds (or pore throats) divided by the volume of the model).

Table 1- Primary (depositional) and diagenetic parameters used in the pore-scale modelling.

Parameter	Notation	Range and Units
Number of bifurcations (branches)	b	1, 2, 3
Shrub width angle	a	20^{o}, 25^{o}, 30^{o}, 35^{o}
Shrub width height	h	6 mm, 9 mm
Cement crust thickness	c	100 µm
Depth of dissolution	ad	100 µm, 150 µm, 200 µm
Percentage of dissolution	asp	40%, 50%, 60%

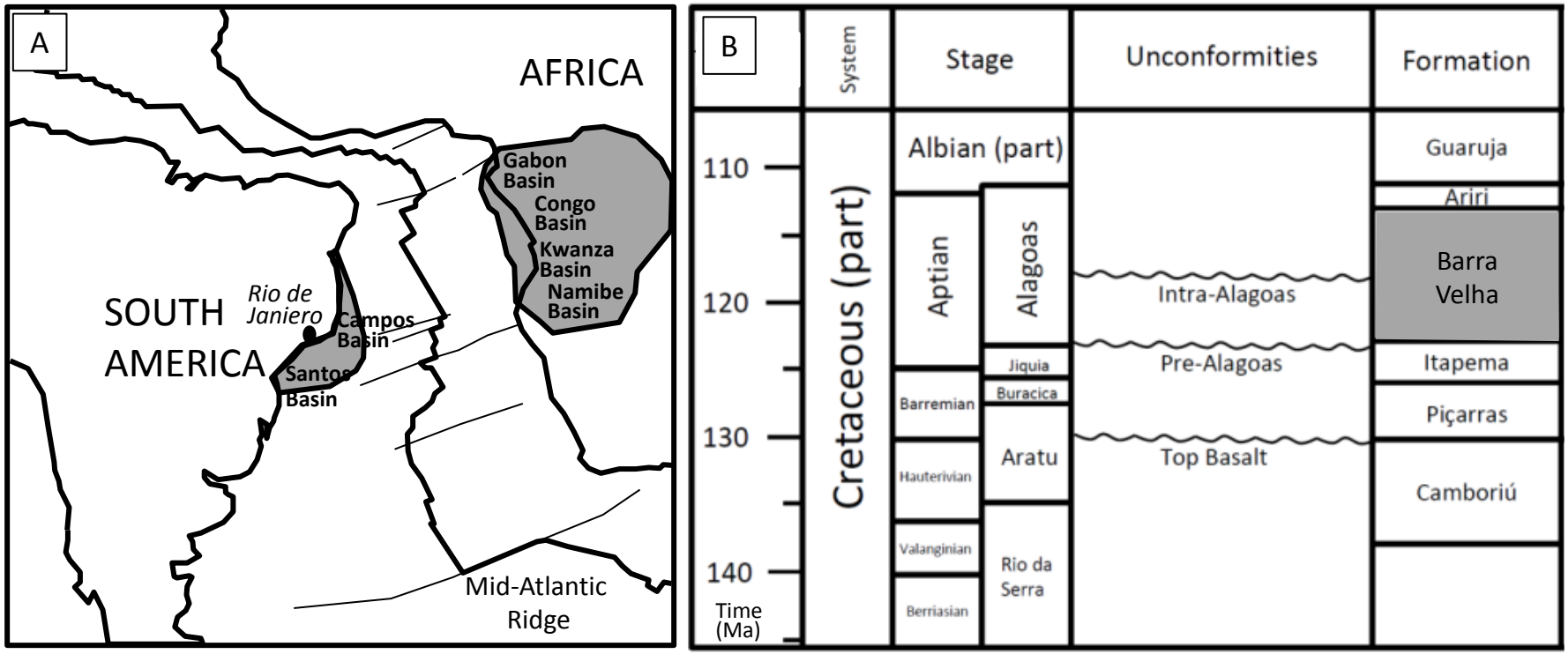
A
AFRICA
Gabon Basin
Congo Basin
Kwanza Basin
Namibe Basin
SOUTH AMERICA
Rio de Janiero
Campos Basin
Santos Basin
Mid-Atlantic Ridge
B
System
Stage
Unconformities
Formation
110
120
130
140
Time (Ma)
Cretaceous (part)
Albian (part)
Aptian
Barremian
Hauterivian
Valanginian
Berriasian
Alagoas
Jiquia
Buracica
Aratu
Rio da Serra
Intra-Alagoas
Pre-Alagoas
Top Basalt
Guaruja
Ariri
Barra Velha
Itapema
Piçarras
Camboriú

Figure 1

Depositional model parameter: shrub **height (h)**

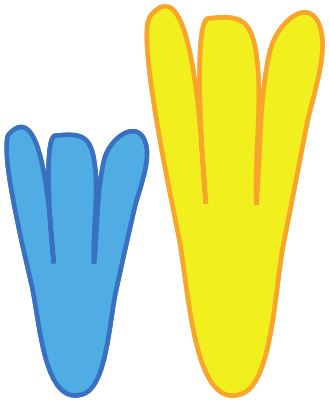

6mm 9mm

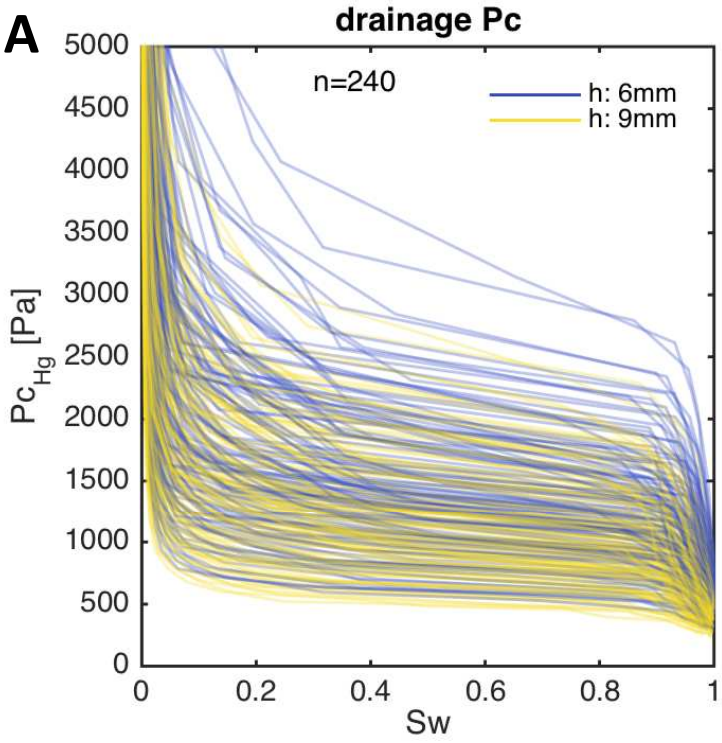

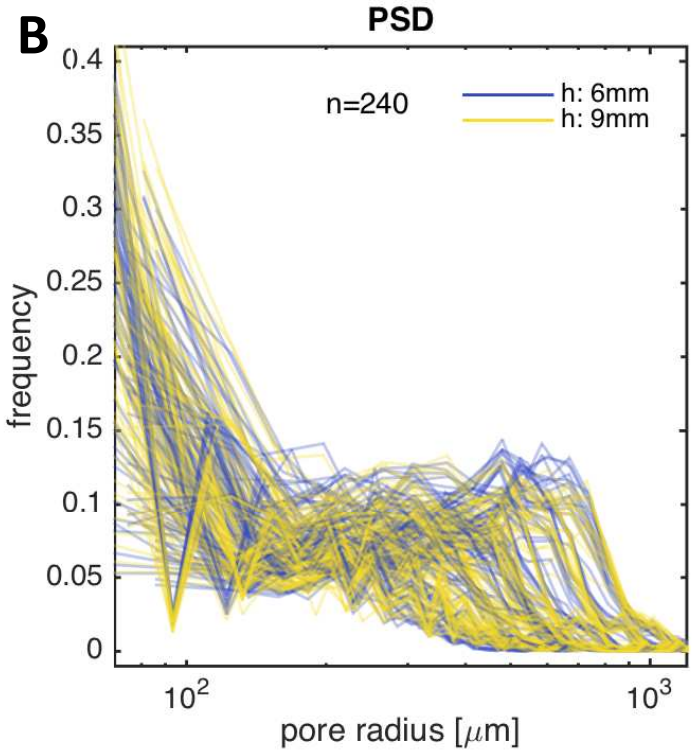

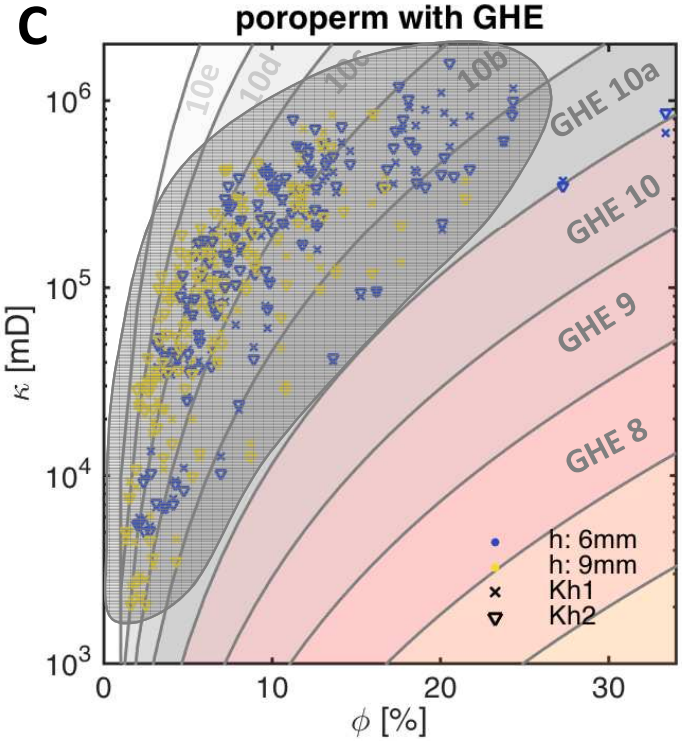

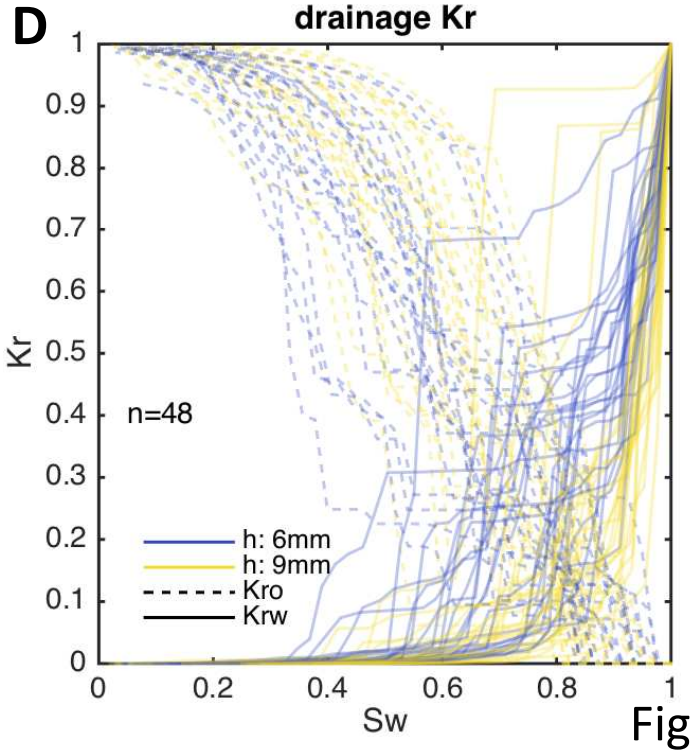

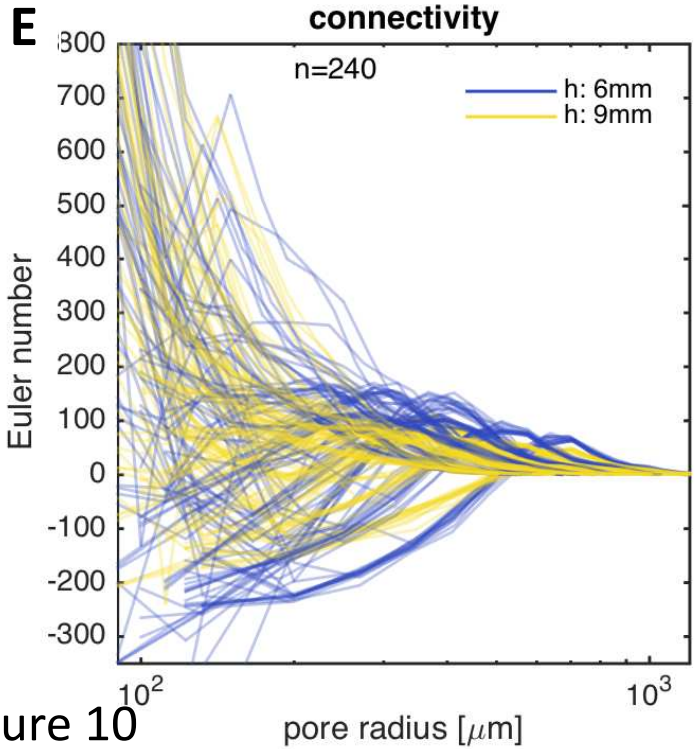

Figure 10

Diagenetic (dissolution) model parameter: **asperity (ad) depth of dissolution**

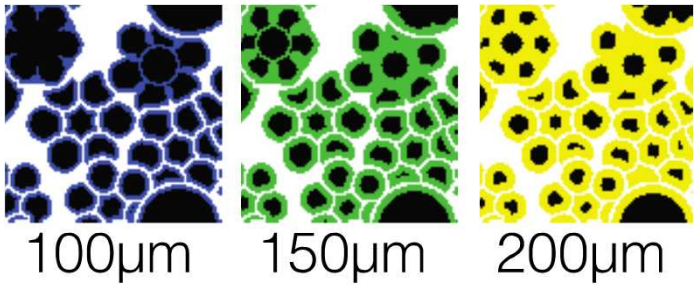

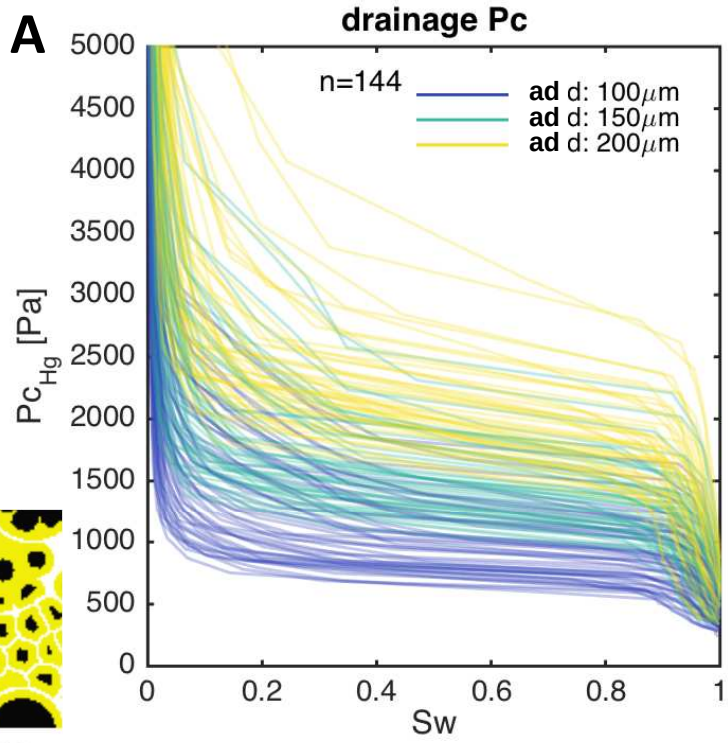

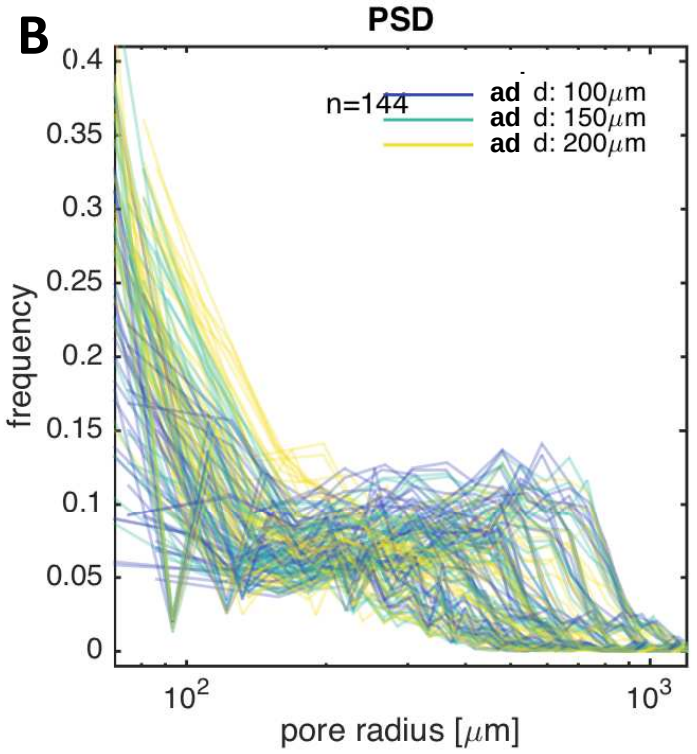

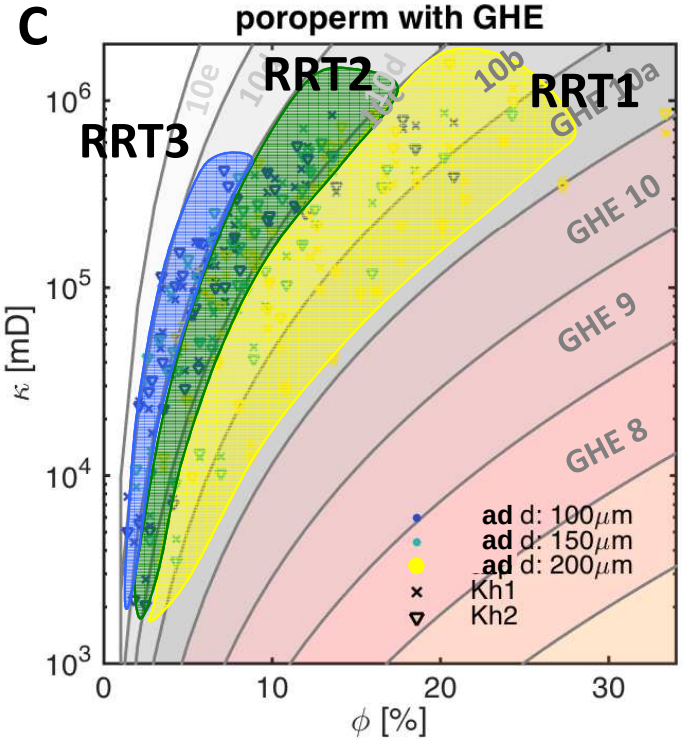

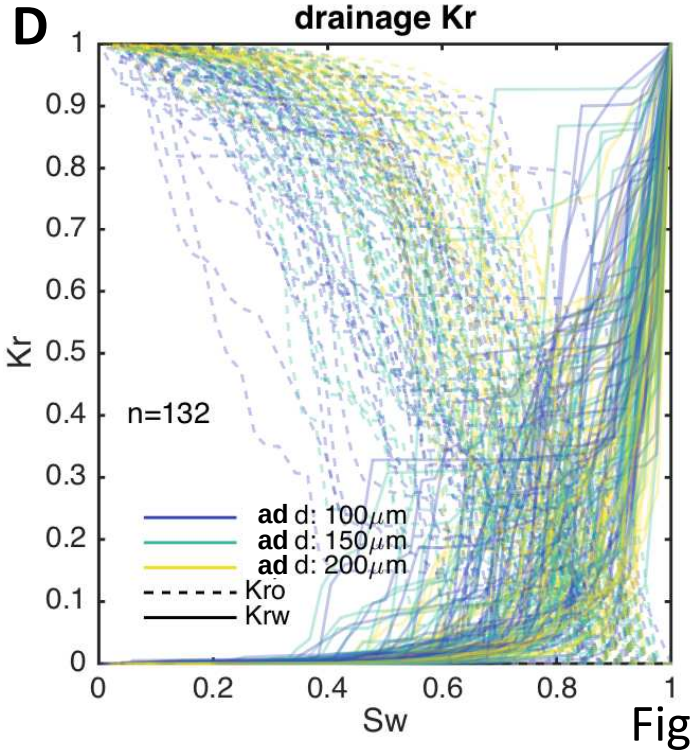

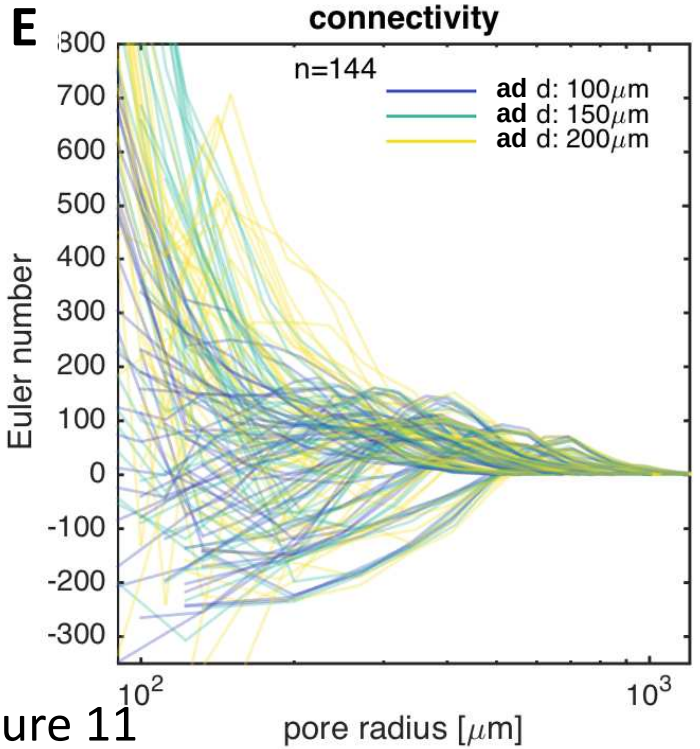

Figure 11

Diagenetic (dissolution) model parameter: **Asperity (asp) percentage of solids removed**

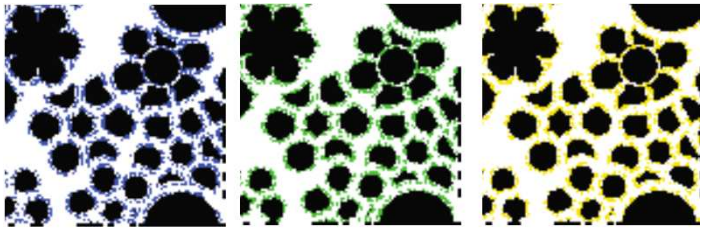

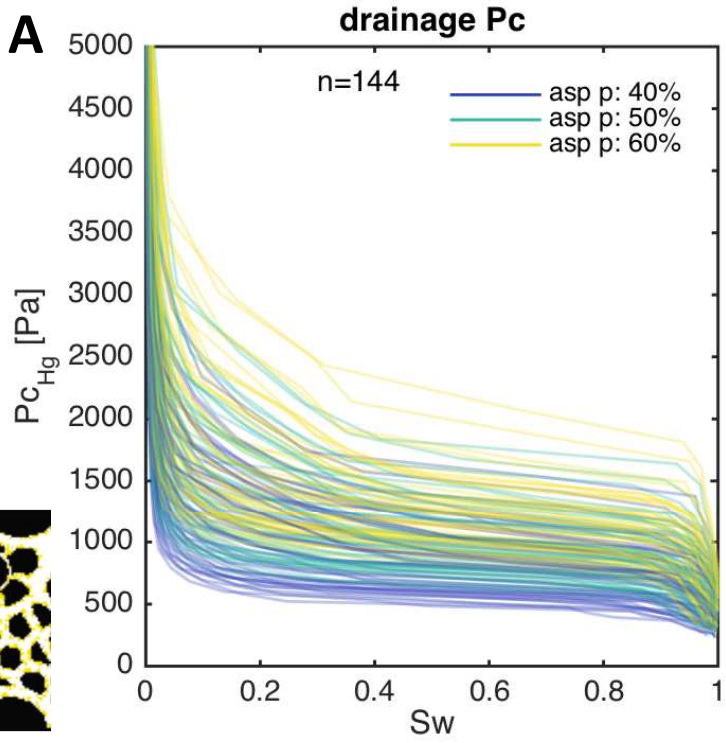

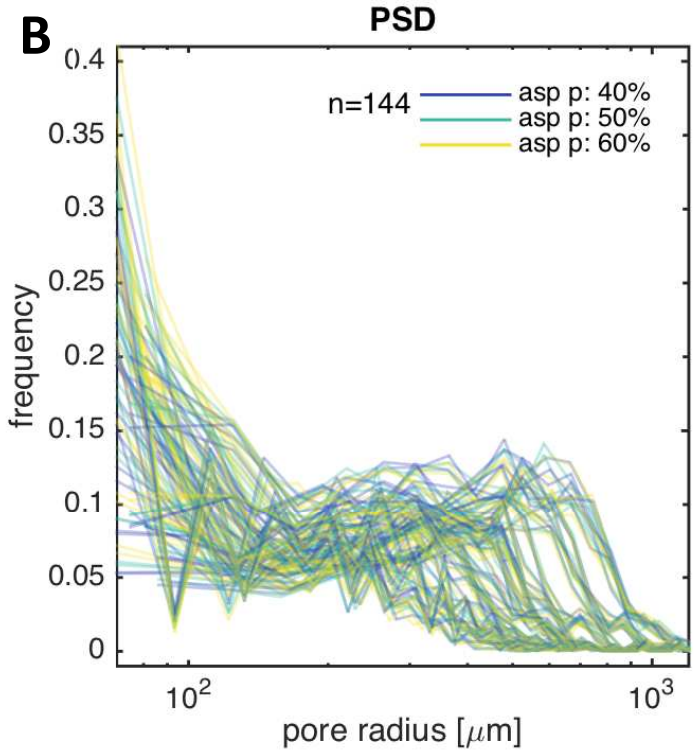

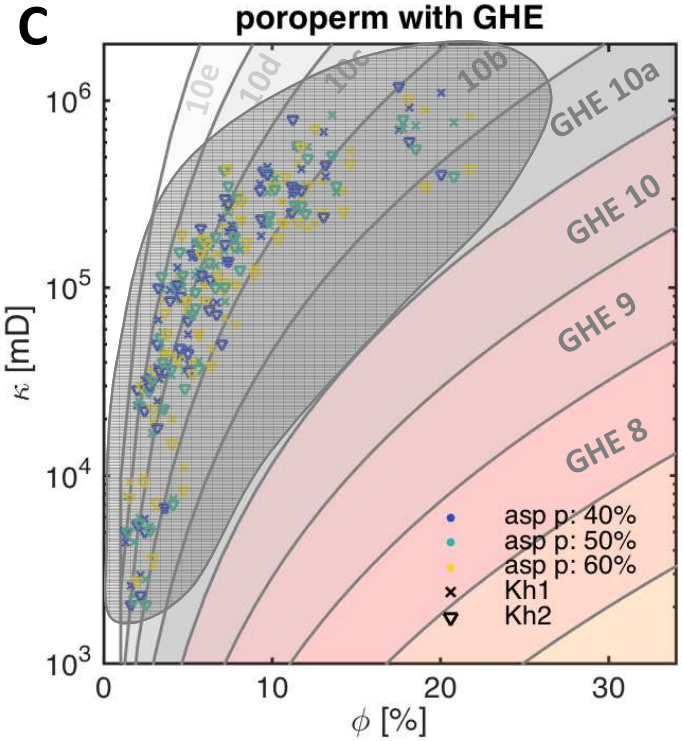

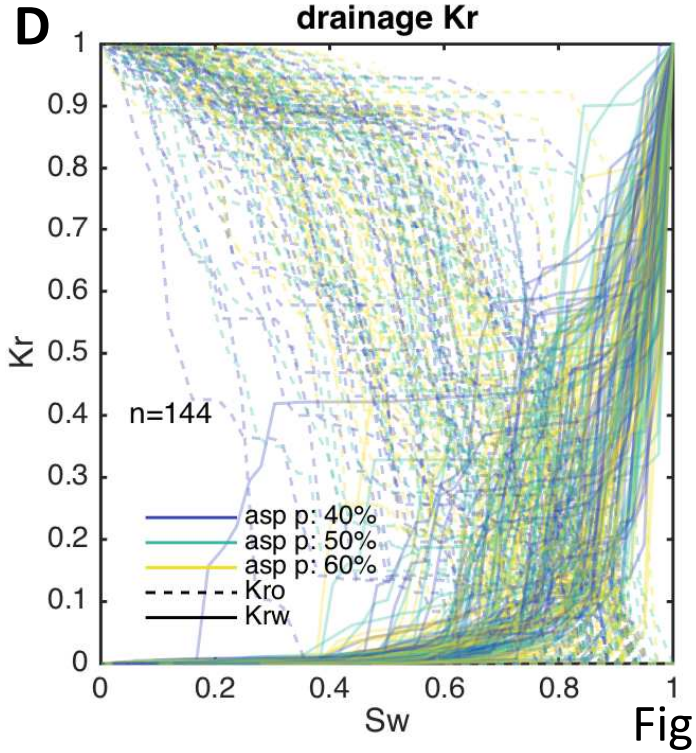

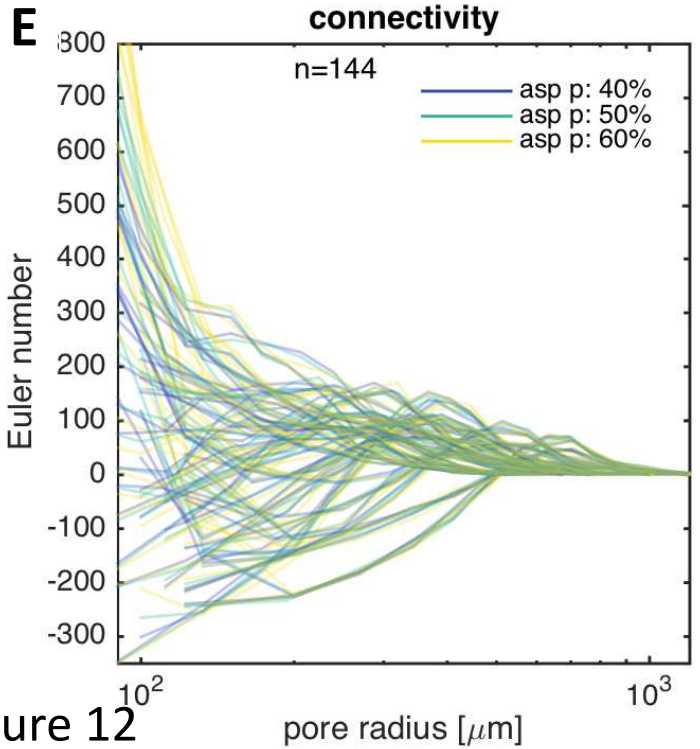

Figure 12

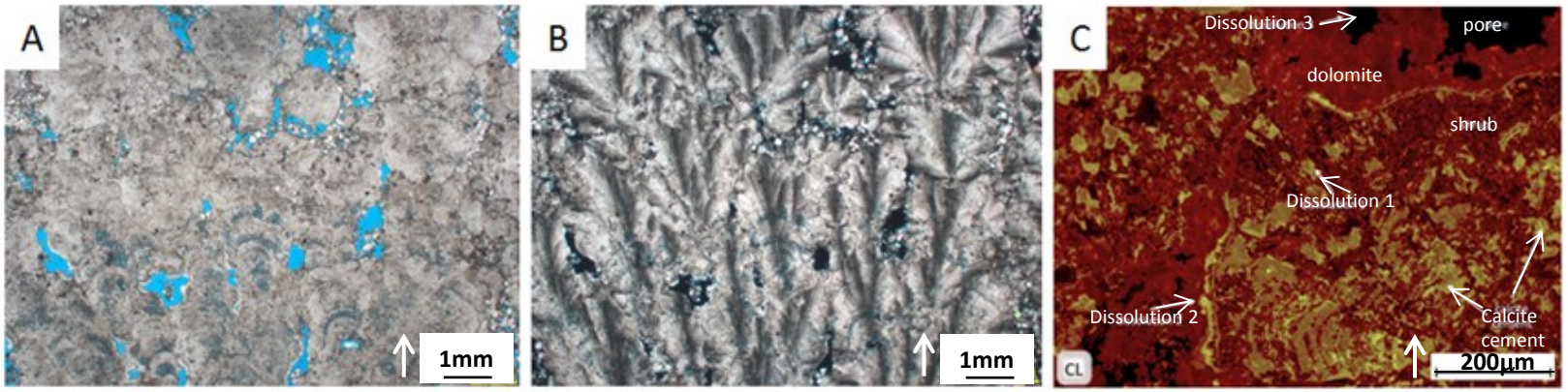
A
1mm
B
1mm
C
Dissolution 3
pore
dolomite
shrub
Dissolution 1
Dissolution 2
Calcite
cement
200µm
CL

Figure 2

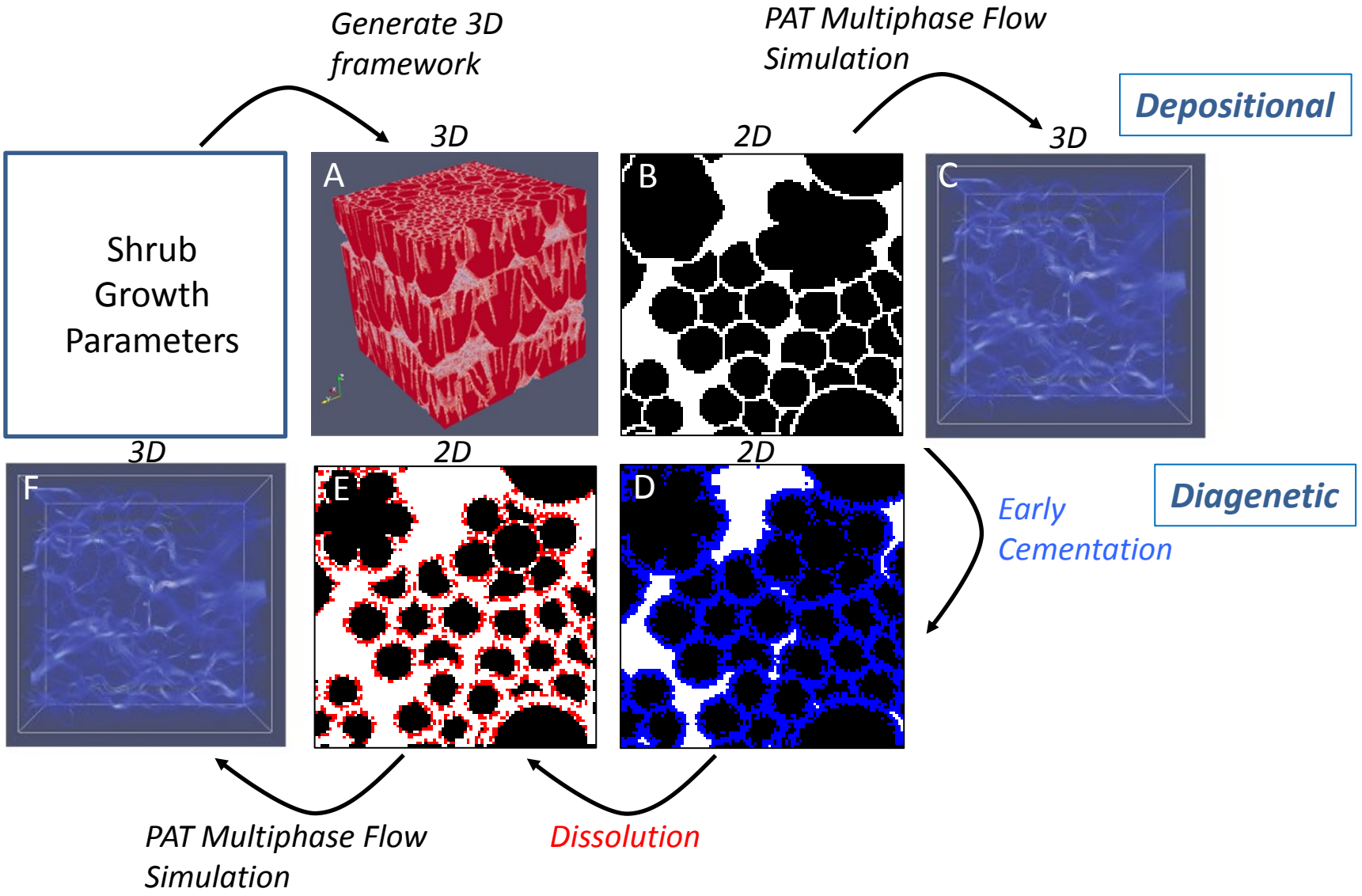
Generate 3D framework
PAT Multiphase Flow Simulation
Depositional
Shrub Growth Parameters
3D
2D
3D
A
B
C
3D
2D
2D
F
E
D
Diagenetic
Early Cementation
PAT Multiphase Flow Simulation
Dissolution

Figure 3

- Average distance between nucleation points (**d**)
- Size of the shrub growth cone (angle **a**)
- Height of the shrub (**h**)
- Number of shrub branch generations (**b**)

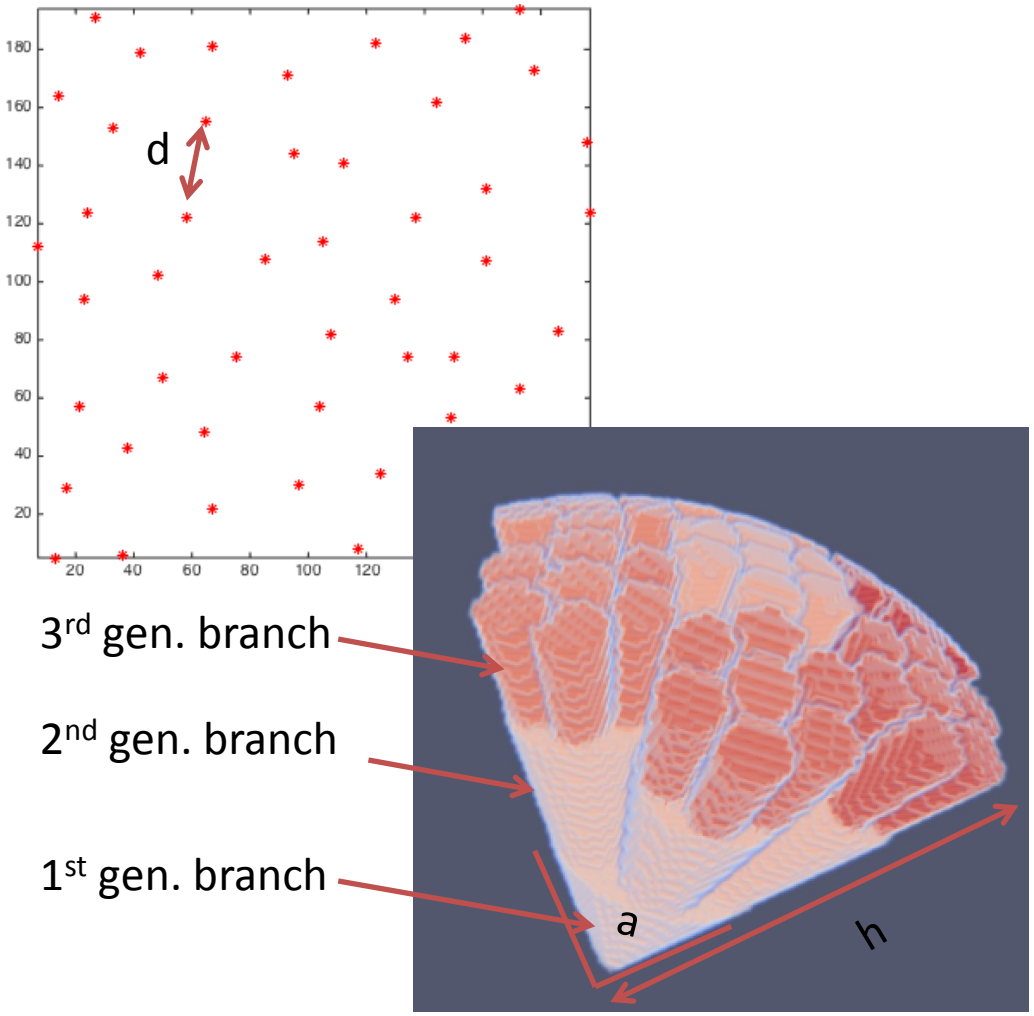

Figure 4

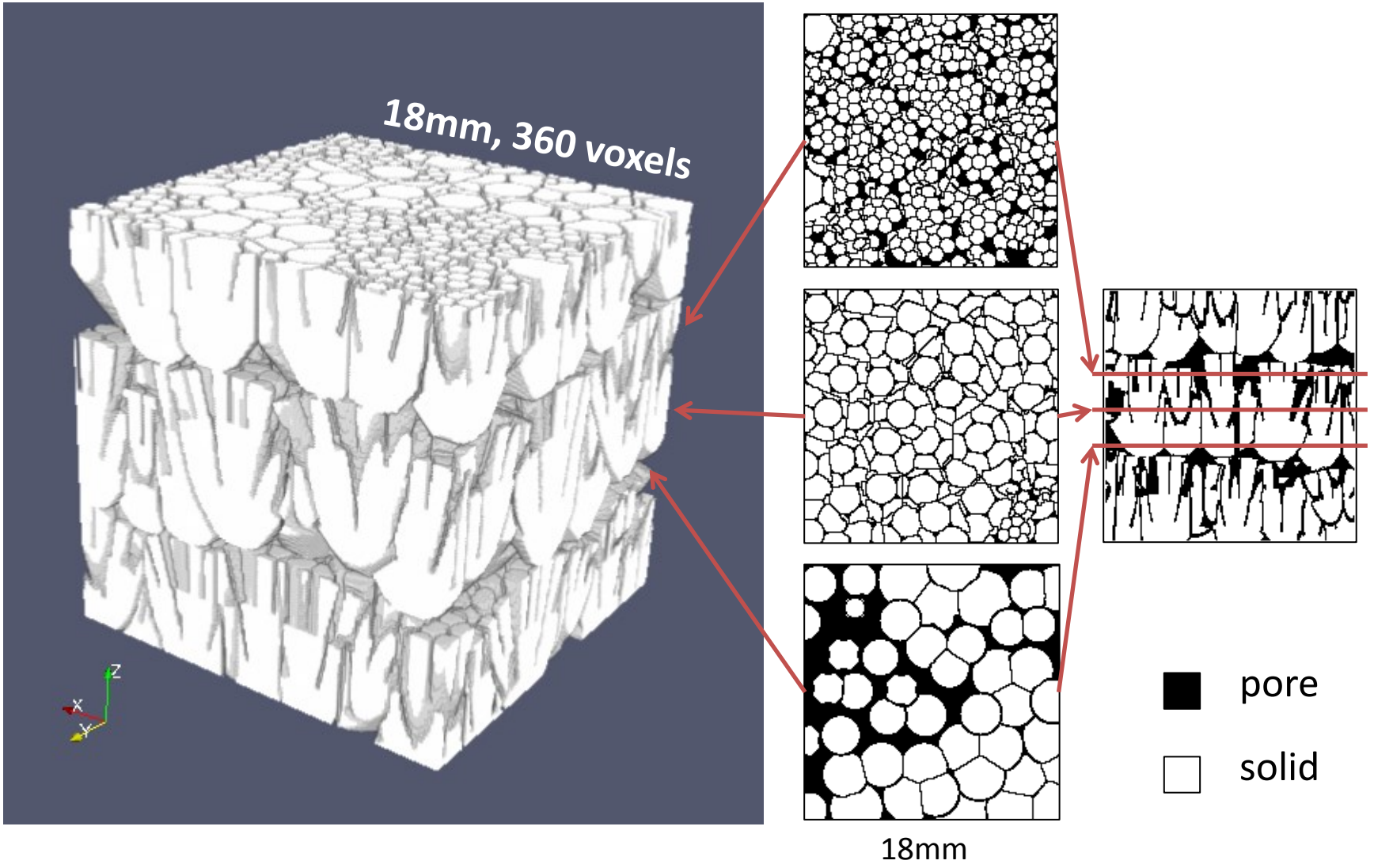

Figure 5

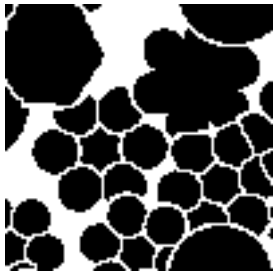

Grown shrub
(cross section)
φ: 41.6%

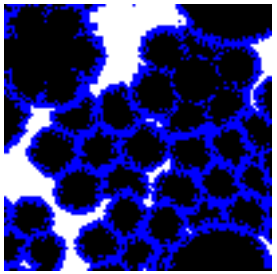

Cementation
(cross-section)
φ: 24.6%

Figure 6

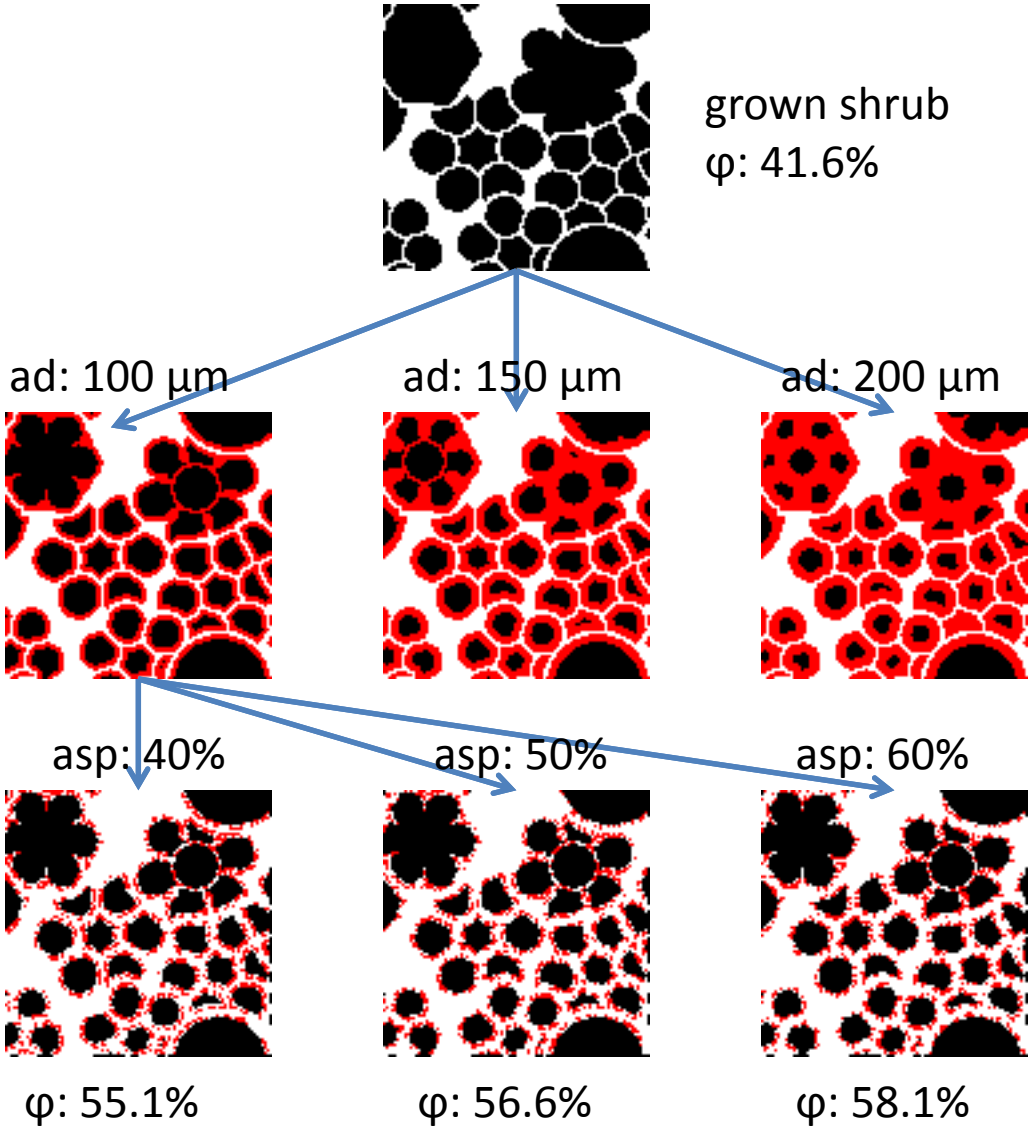
grown shrub
φ: 41.6%
ad: 100 μm
ad: 150 μm
ad: 200 μm
asp: 40%
asp: 50%
asp: 60%
φ: 55.1%
φ: 56.6%
φ: 58.1%

Figure 7

Depositional model parameter: shrub width **angle (ang)**

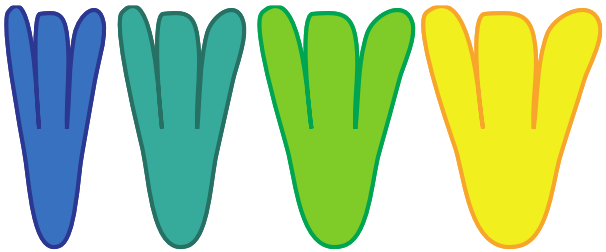

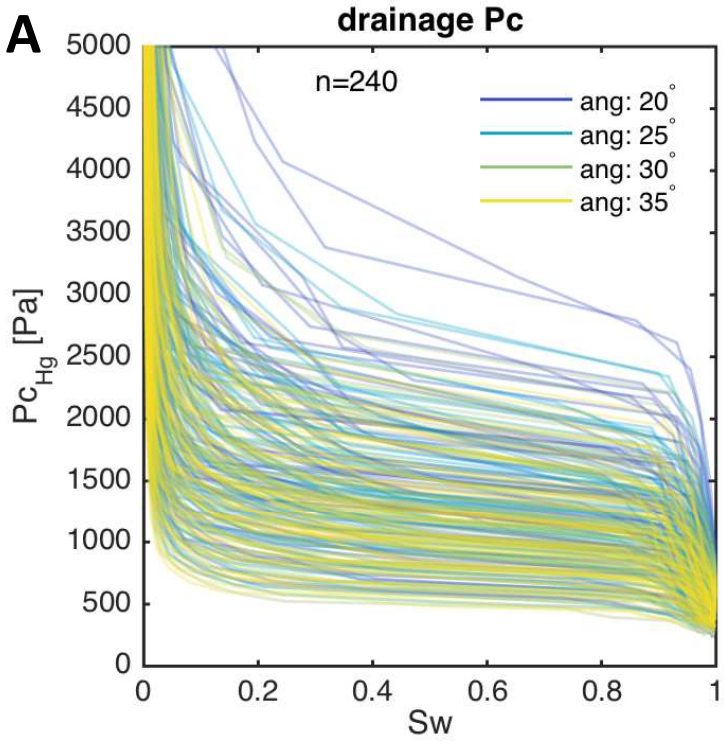

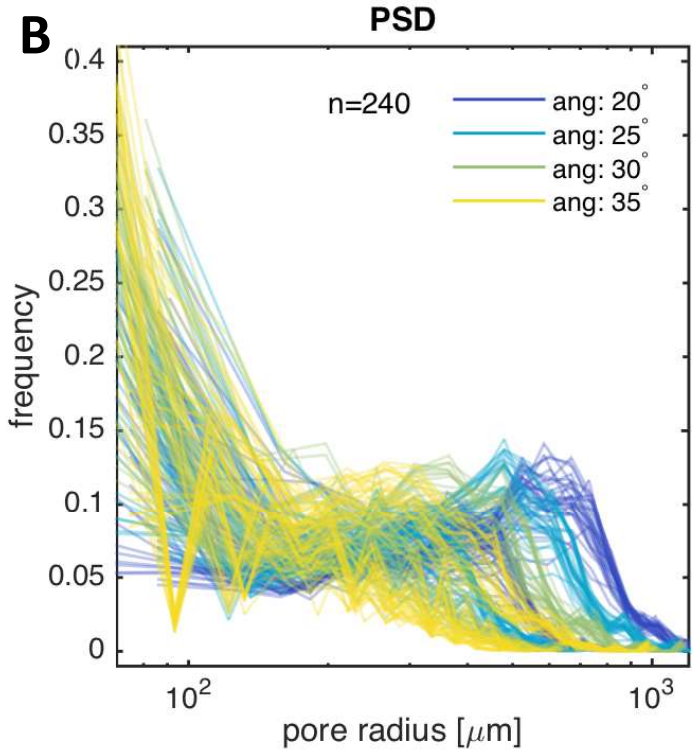

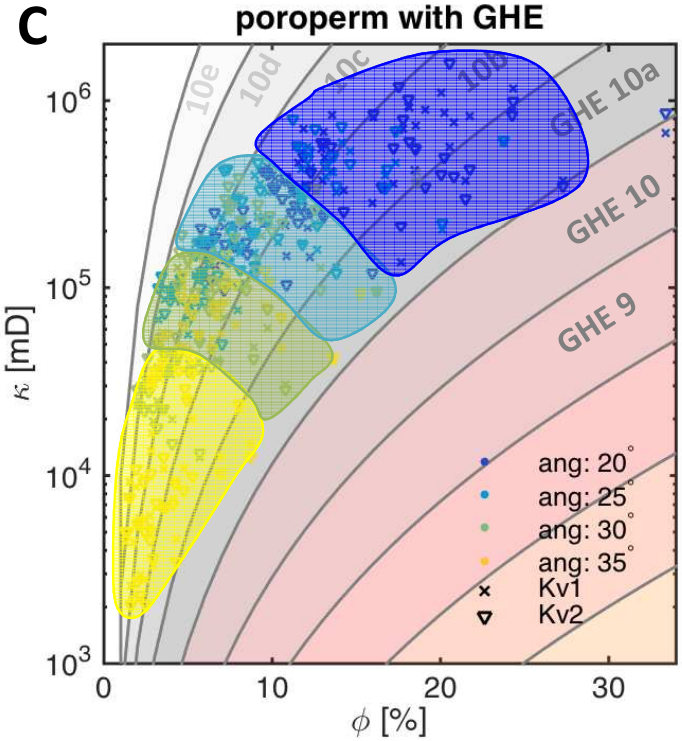

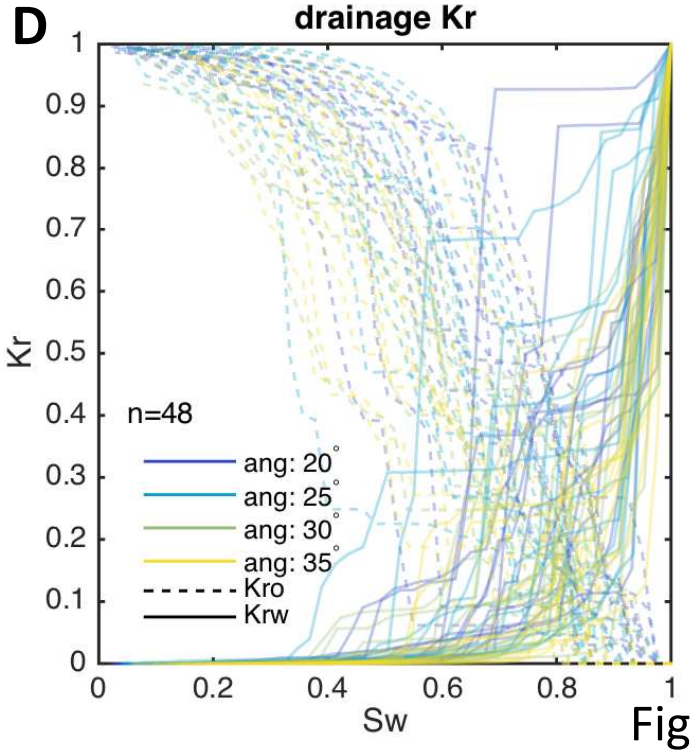

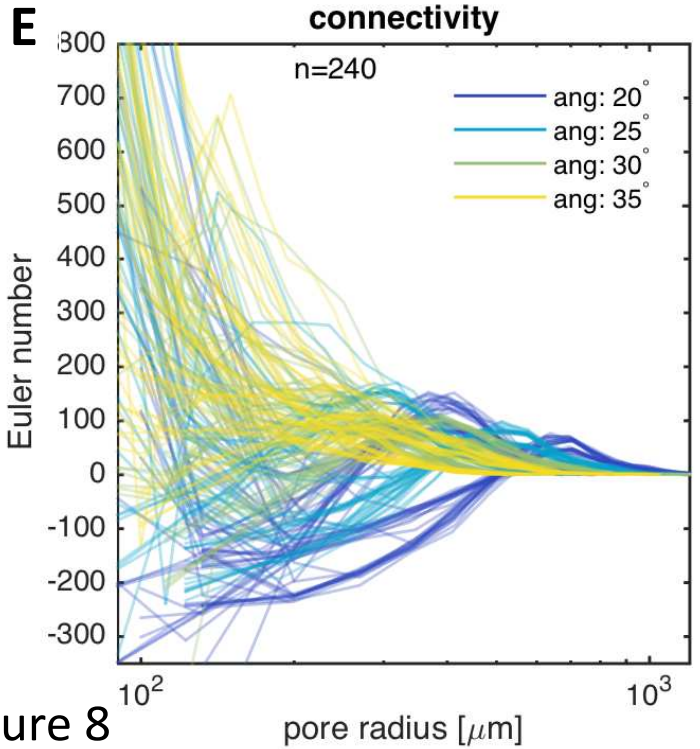

Figure 8

Depositional model parameter: shrub degree of **Branching (branch)**

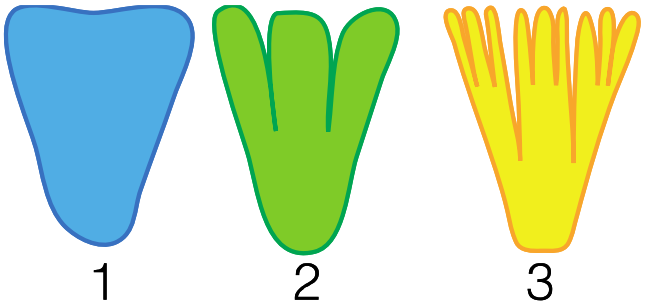

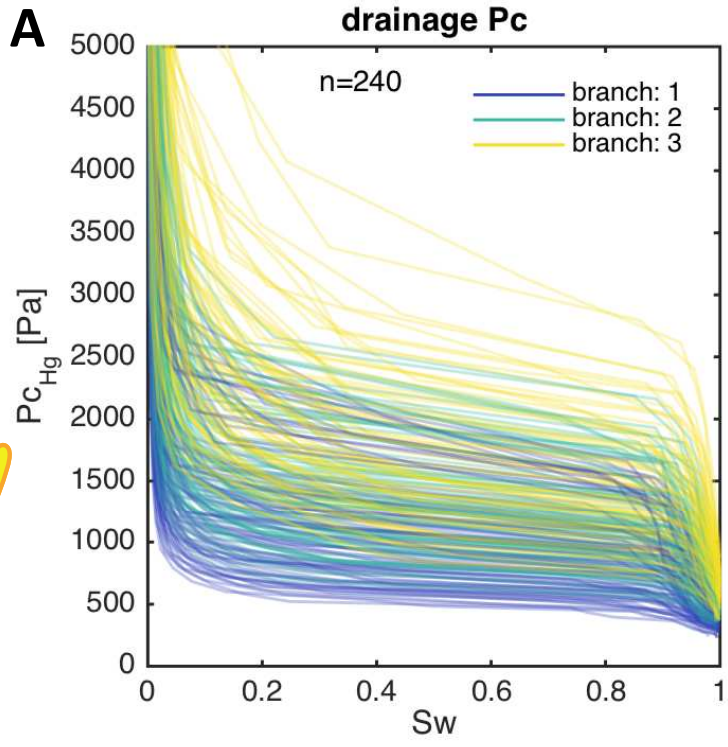

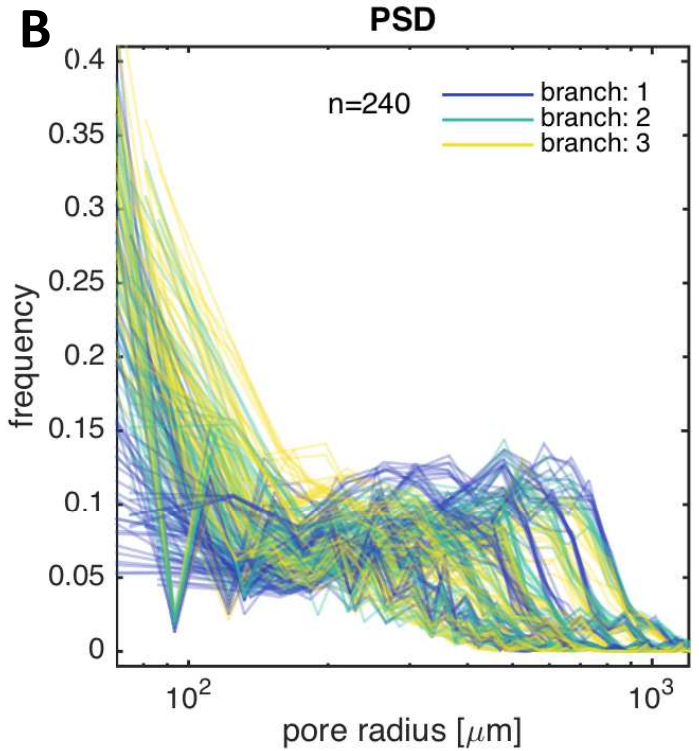

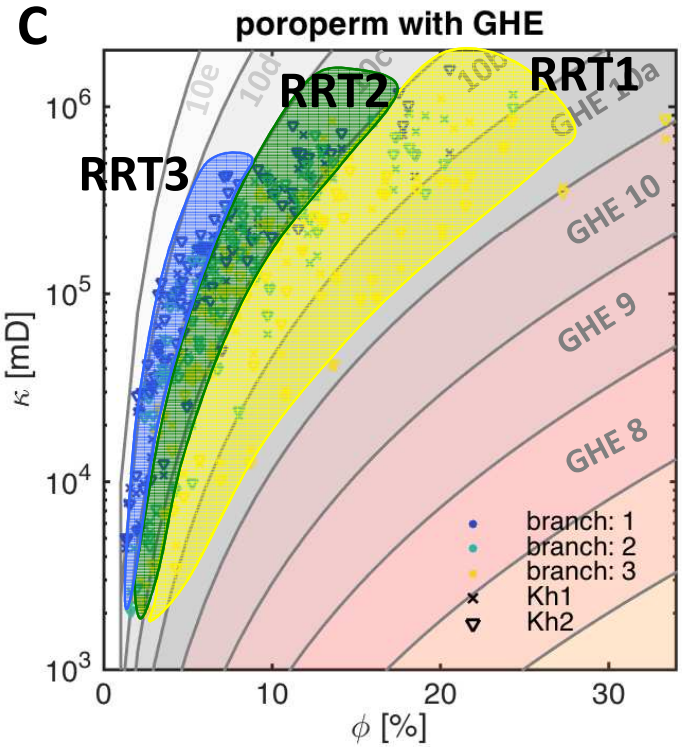

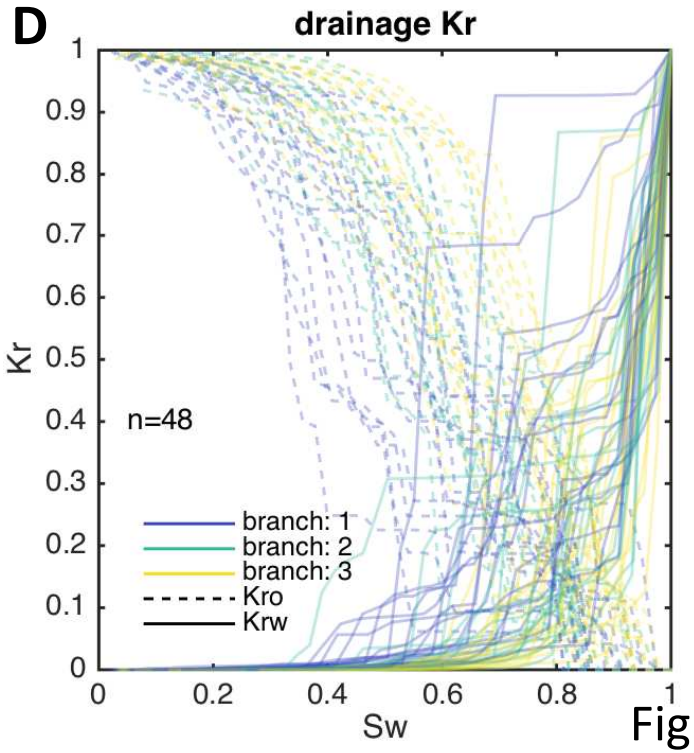

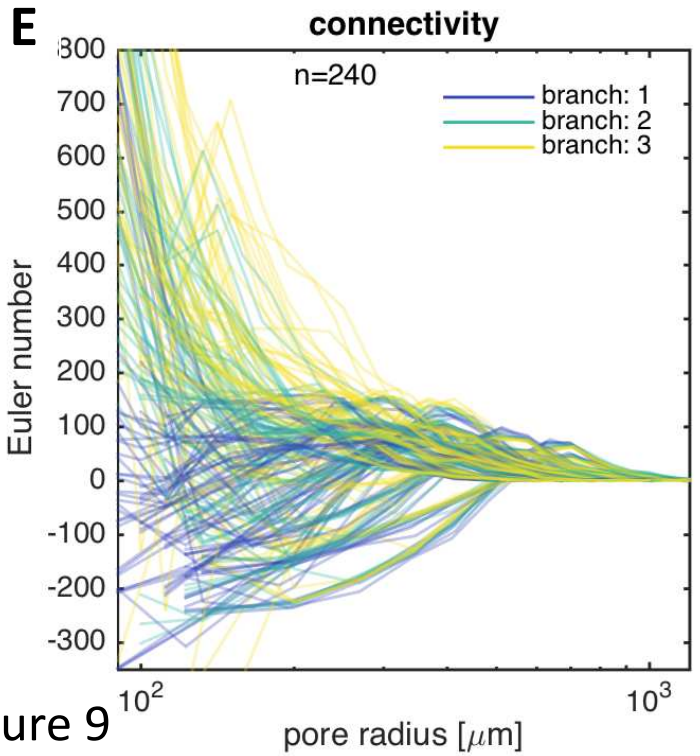

Figure 9

Highlights

We model reservoir flow behaviour of the unusual lacustrine Pre-Salt crystal-shrub limestones of the Cretaceous Santos Basin, Brazil. Rather than producing models validated to actual reservoir properties, we seek to establish the impact of depositional and diagenetic parameters and identify shared petrophysical behaviour.

Simulations show that the number of shrub bifurcations and the degree of dissolution follow established Kozeny-Carman (KC) porosity-permeability relationships. By contrast, the angle of shrub inflation produces data clusters that traverse KC bands. These trends provide guidance for potential rock type subdivision of similar lithologies. We propose that the crystal-shrub limestones can be subdivided into three broad petrophysical rock types based on the degree of shrubby aggregate bifurcation and extent of dissolution.

The trends explored here can be used to link conceptual and process-based geological models to data, so enabling more accurate prediction and upscaling of heterogeneous reservoir properties and their reservoir-scale distribution.

Declaration of interests

☒ The authors declare that they have no known competing financial interests or personal relationships that could have appeared to influence the work reported in this paper.

☐The authors declare the following financial interests/personal relationships which may be considered as potential competing interests: